Chapter 4

Quantifying Three-Dimensional Deformations of Migrating Fibroblasts

This chapter presents the full-field displacements and tractions of 3T3 fibroblast cells during migration on polyacrylamide (PA) substrates of varying stiffness. The notation of a *soft* substrate corresponds to a Young's modulus of the polyacrylamide gel of ~ 0.82 kPa, whereas *stiff* denotes a Young's modulus of ~ 9.64 kPa as presented in Chapter 3. While the displacement fields are calculated on a uniformly spaced Cartesian grid given by the DVC algorithm, the cell's orientation oftentimes does not follow a principal Cartesian coordinate direction. Hence, due to the finite grid spacing used in the DVC calculations (8 voxels or ~ 2 μm) interpolation may be necessary to determine the displacement and strain field values for an arbitrary orientation. The data presented here are interpolated only as necessary between grid points utilizing primarily a trilinear scheme. Occasionally tricubic interpolation is utilized to better resolve steeper gradients, though trilinear interpolation is generally preferred since it introduces less data smoothing. However, for additional computational cost the DVC grid spacing could be reduced to a minimal value of 1 voxel. Yet this cost is enormous (on the order of days to weeks per volume stack), and hence is not performed within the scope of this study.

4.1 Three-Dimensional Displacements and Tractions

This section defines the displacement and traction notations that will be used throughout the chapter. It also describes how cell applied tractions are calculated. Chapter 2 described in depth how the three-dimensional displacements and the associated strains are calculated. All of the calculated and presented displacements, tractions and surface normals are referenced to the generalized Cartesian coordinates x_1, x_2, x_3.

4.1.1 Definition of the Three-Dimensional Displacement Vector

The three-dimensional displacement vector $\mathbf{u}$, having components u_1, u_2, and u_3, is defined as

$$\mathbf{u} = \begin{pmatrix} u_1 \\ u_2 \\ u_3 \end{pmatrix}, \tag{4.1}$$

with its magnitude given by

$$|\mathbf{u}| = \sqrt{u_1^2 + u_2^2 + u_3^2}. \tag{4.2}$$

4.1.2 Traction Calculations

Chapter 3 presented the material characterization of the polyacrylamide gels, and it was experimentally shown that these can be reasonably treated as isotropic, linearly elastic, incompressible, time-independent materials for the context of the here presented study. At each time increment the cell-induced strains were computed and it was found that the strains were within the linear range of the material behavior, in particular, the strain magnitudes per time increment were consistently found to be less than 5%. Chapter 2 described how the strain tensor is calculated, which will be denoted here as $\boldsymbol{\epsilon}$.

In order to calculate traction stresses including surface tractions, the stress tensor $\boldsymbol{\sigma}$ needs to be

determined first, and is calculated, based on the above constitutive properties as

$$\boldsymbol{\sigma} = 2\mu\boldsymbol{\epsilon}, \tag{4.3}$$

where μ is the shear modulus, which is related to Young's modulus E and to Poisson's ratio ν by

$$E = 2\mu(1+\nu). \tag{4.4}$$

Calculation of the traction stresses involves using the well-known Cauchy relation

$$\mathbf{T} = \boldsymbol{\sigma} \cdot \mathbf{n}, \tag{4.5}$$

where $\mathbf{T}$ is defined as the three-dimensional traction vector, and $\mathbf{n}$ is the surface normal of an arbitrary plane on which $\mathbf{T}$ acts given by

$$\mathbf{T} = \begin{pmatrix} T_1 \\ T_2 \\ T_3 \end{pmatrix}, \tag{4.6}$$

and

$$\mathbf{n} = \begin{pmatrix} n_1 \\ n_2 \\ n_3 \end{pmatrix}. \tag{4.7}$$

The magnitude of the three-dimensional traction vector is then defined as

$$|\mathbf{T}| = \sqrt{T_1^2 + T_2^2 + T_3^2}. \tag{4.8}$$

All tractions are presented in units of $pN/\mu m^2$ or Pascal (Pa), and can also be represented as a individual traction forces per unit area.

4.2 Three-Dimensional Cell-Induced Displacements During Cell Migration on Soft Substrates

Full-field displacement measurements were carried out using the LSCM-DVC technique applied to migrating 3T3 Fibroblast cells on soft polyacrylamide gels. The results shown here represent the cell-induced deformation fields that were observed tracking single cells over an extended period of time. Confocal volume stacks were recorded at 35 min time increments, while each cell was tracked over several hours. Further details of the imaging conditions including the size of the imaged volumes is described in Chapter 3. Time t_0 denotes the start point of each experiment, whereas t_1 describes the first 35 min time increment. Altough the initial cell spreading time history was not recorded, the results display snapshots of the dynamic interactions between the single fibroblast cell and the substrate. The substrate thickness for the subsequently shown results is 40 μm. In order to reduce the effects of phototoxicity and photobleaching during cell imaging, the imaged confocal volume size was limited to 48% of the total substrate thickness. As the subsequent Figs. show, this volume size is sufficient to capture most of the cell-induced deformation field within the resolution limits of the technique. The LSCM-DVC method is able to detect displacement changes greater than 0.12 μm, where 0.12 μm was determined to be the sensitivity threshold through baseline tests. These baseline tests consist of the same material and experimental setup but without any cells present, which allows establishing the measurement sensitivity.

The cell is visualized simultaneously with the displacement of the fluorescent particles inside the polyacrylamide gels using two separate photodetectors. This procedure allows correlating the position of the cell determined by the GFP-actin fluorescent marker construct with the substrate displacement field. GFP-actin highlights the actin filaments of the cell, which are one of the three main structural filaments comprising a cell. Therefore, GFP-actin can be used the visualize the shape of the cell during the migration increments. However, due to the finite life-time of the fluorescent protein marker used to visualize the cell shape, occasionally parts of the cell are not visible at locations where considerable deformations are observed.

Figure 4.1 shows a time evolution of the surface displacement fields beneath a migrating cell over a time span of 140 min. The color contour plots display the magnitude of the three-dimensional displacement vector $|\mathbf{u}|$ in μm. The linear dimension of the cell along its major axis in all of the plots is approximately 100 μm. The direction of cell migration is from the left to the right. The cell migration speed, as determined by tracking the nucleus of the cell, is $\approx$ 18 μm/hr, which is within the range of reported fibroblast migration speeds on polyacrylamide gels [29].

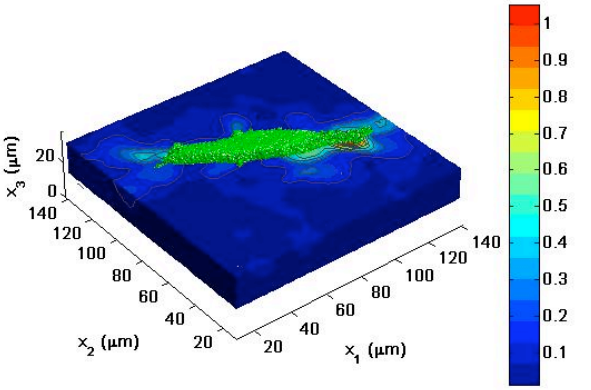

(a) Cell-induced surface displacements at $t_1 = 35$ min

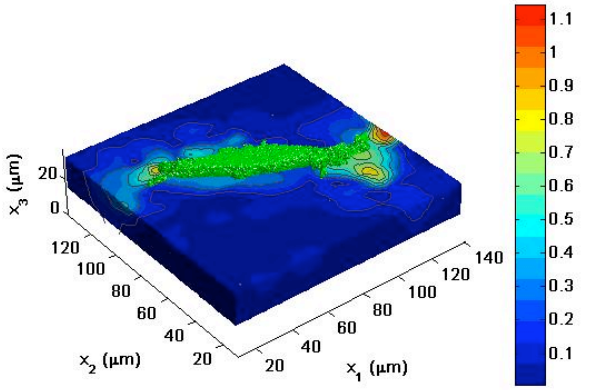

(b) Cell-induced surface displacements at $t_2 = 70$ min

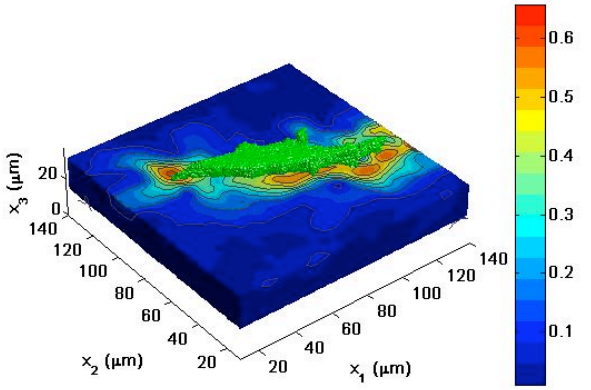

(c) Cell-induced surface displacements at $t_3 = 105$ min

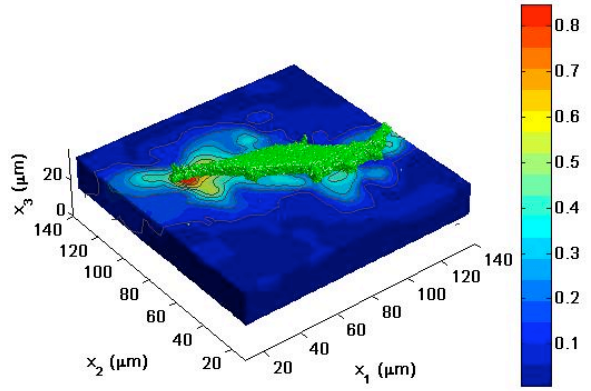

(d) Cell-induced surface displacements at $t_4 = 140$ min

Figure 4.1: Surface contour plots of the magnitude of the three-dimensional displacement vector during cell migration. The color bar represents the magnitude of the total three-dimensional displacement vectors in μm, and the cell (green) is superimposed on the three-dimensional contour plots to show its position with respect to the deformation field.

Figure 4.2 shows the time evolution of the displacement field along an arbitrary slice beneath the migrating cell's long axis over a time span of 140 min. Here the decay of the magnitude of the three-dimensional displacement vectors are shown for the same time series as in Fig. 4.1. The color contour plots display the magnitude of the three-dimensional displacement vector in μm. The displacement contour slices highlight the dynamic interaction of the cell with its substrate as characterized by changes in magnitudes and location of the observed displacements.

Figure 4.3 examines the displacement field of the arbitrary planar slice in Fig. 4.2(a) in more detail. Figure 4.3(a) shows the magnitude of the three-dimensional displacement vector as color contours along the same planar slice, while the white arrows represent the (u_3, u_1) displacement components. The color bar displays the units in μm, whereas the magnitude of the longest arrow corresponds to 0.8 μm. Figure 4.3(b) plots an enlarged picture of Fig. 4.3(a) highlighting an arbitrarily chosen location to generate a line profile of each displacement component as a function of depth (x_3), which is shown in Fig. 4.3(c). While the overall displacement magnitude decays approximately as $x_3^{3/2}$, the magnitude of the individual displacement components highlights the importance of the u_3 component at that particular time increment (t_1).

Figure 4.4 displays the displacement distribution along the same arbitrary plane as in Fig. 4.3 for the next time increment $t_2 = 70$ min. Figure 4.4(a) shows the magnitude of the three-dimensional displacement vector as color contours along the same planar slice, while the white arrows represent the (u_3, u_1) displacement components. The color bar displays the units in μm, whereas the magnitude of the longest arrow corresponds to 0.8 μm. Figure 4.3(b) plots an enlarged picture of Fig. 4.3(a) highlighting an arbitrarily chosen location to generate a line profile of each displacement component as a function of penetration depth (x_3), which is shown in Fig. 4.3(c). The displacement contour and line profiles show a slower decay with thickness than presented in Fig. 4.3 at time t_1.

Figures 4.5 and 4.6 display the surface displacement fields presented in Figs. 4.1(a) and 4.1(b) in more detail. In particular, Fig. 4.5(a) shows the magnitude of the three-dimensional displacement vector as color contours directly underneath the migrating cell, while the white arrows represent the $\{u_1, u_2\}$ displacement components. The color bar displays the units in μm, whereas the magnitude

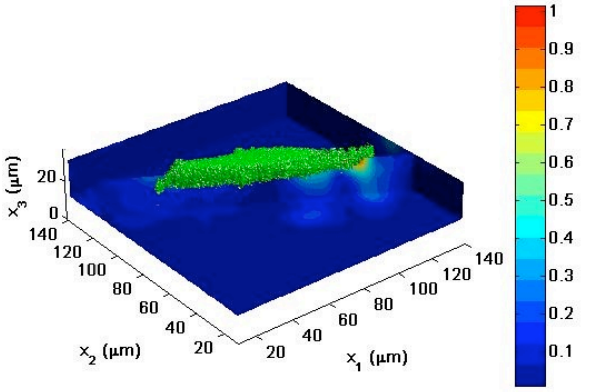

(a) Cell-induced displacements at $t_1 = 35$ min

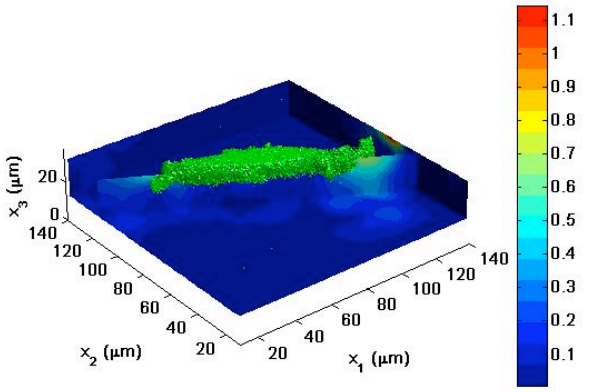

(b) Cell-induced displacements at $t_2 = 70$ min

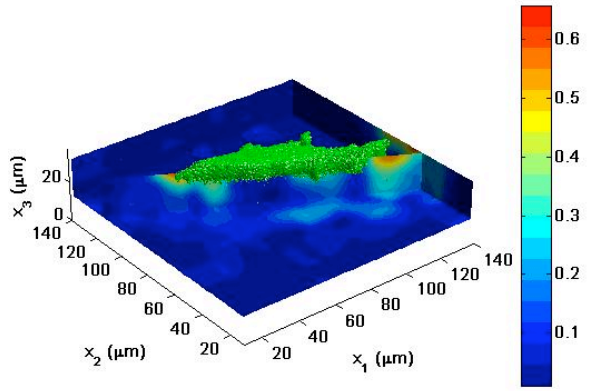

(c) Cell-induced displacements at $t_3 = 105$ min

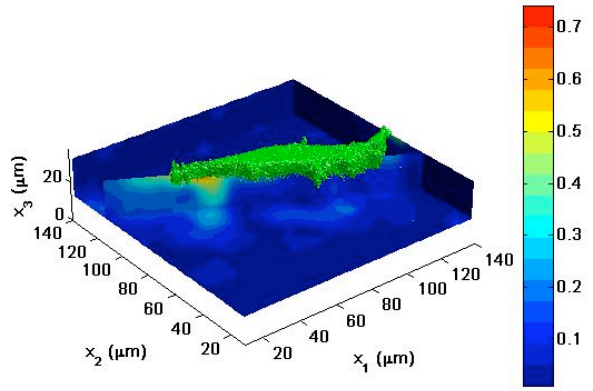

(d) Cell-induced displacements at $t_4 = 140$ min

Figure 4.2: Arbitrary displacement contour slices along the long axis of the cell. The slices of displacement contours underneath migrating cells show significant deformation in the normal plane that decay along the thickness of the sample. The two edges in the image are included to show that there are negligible displacements detected from neighboring cells (contours are dark blue). The color bar represents the magnitude of the total three-dimensional displacement vectors in μm, and the cell (green) is superimposed on the three-dimensional contour plots to show its position with respect to the deformation field.

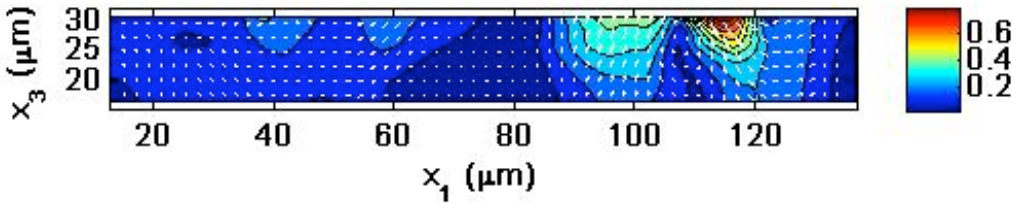

(a) Cross-sectional displacement contour plot through the substrate thickness at $t_1 = 35$ min

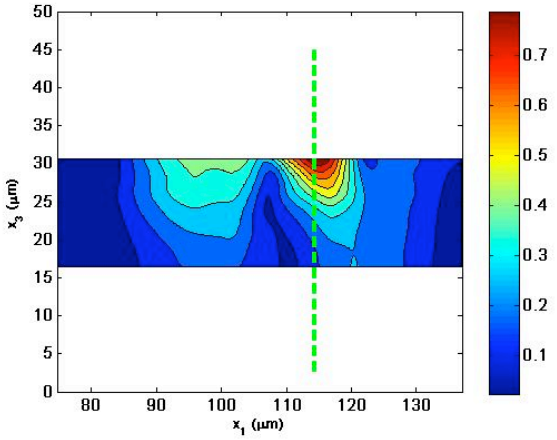

(b) Enlarged view of the contour plot in 4.3(a) and location of displacement line plot shown in 4.3(c)

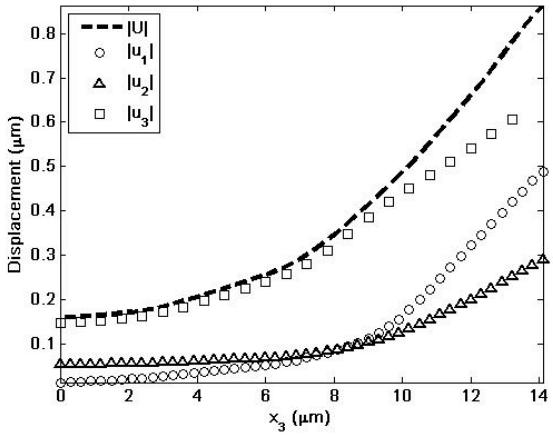

(c) Displacement line profile through the thickness of the gel (x_3). The maximum x_3 value corresponds to the gel surface.

Figure 4.3: Displacement contour and line plot profiles as a function of depth (x_3) through the thickness of the gel. Figure 4.3(a) shows the same displacement contours along the long axis of the cell as shown in Fig. 4.2(a), where the color bar represents the magnitude of the three-dimensional displacement vectors in μm, and the white arrows show the direction of the in-plane (u_1,u_3) displacement components only. Figure 4.3(b) shows the zoom-in image of Fig. 4.3(a), whereas Fig. 4.3(c) illustrates the decay of all three displacement components in the x_3 direction, where $x_3 = 14$ represents the location of the top surface.

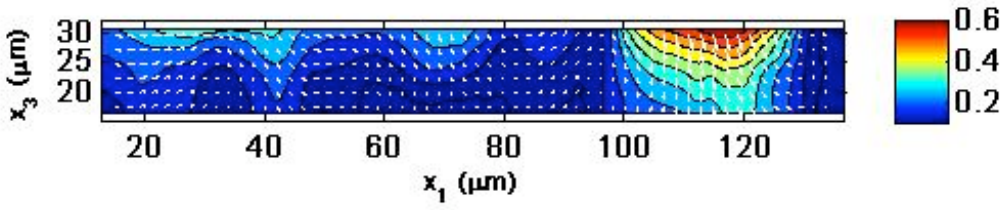

(a) Cross-sectional displacement contour plot through the substrate thickness at $t_2 = 70$ min

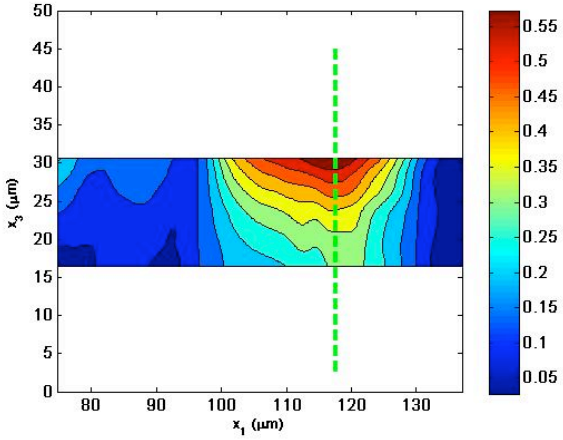

(b) Enlarged view of the contour plot in 4.4(a) and location of displacement line plot shown in 4.4(c)

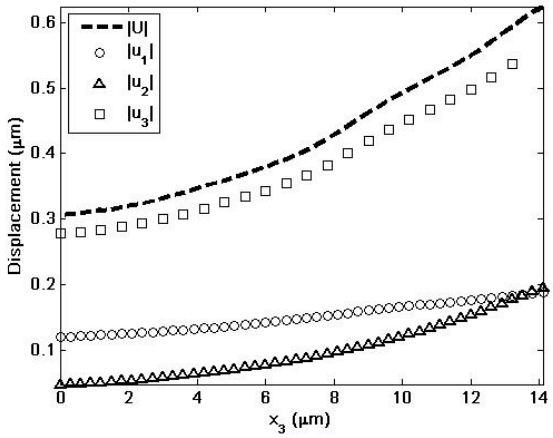

(c) Displacement line profile through the thickness of the gel (x_3). The maximum x_3 value corresponds to the gel surface.

Figure 4.4: Displacement contour and line plot profiles as a function of depth (x_3) through the thickness of the gel. Figure 4.4(a) shows the same displacement contours along the long axis of the cell as shown in Fig. 4.2(b), where the color bar represents the magnitude of the three-dimensional displacement vectors in μm, and the white arrows show the direction of the in-plane (u_1,u_3) displacement components only. Figure 4.3(b) shows the zoom-in image of Fig. 4.3(a), whereas Fig. 4.3(c) illustrates the decay of all three displacement components in the x_3 direction, where $x_3 = 14$ represents the location of the top surface.

of the longest arrow corresponds to 1.6 μm. Figure 4.5(b) plots an enlarged picture of Fig. 4.5(a) highlighting an arbitrarily chosen location to generate a line profile of each displacement component as a function of spatial distance, which is shown in Fig. 4.3(c). Here, the displacement distribution follows an almost Gaussian profile obtaining a maximum value of 1.8 μm over a length of $\sim$ 1 μm, most likely corresponding to the particular location of a focal adhesion complex. As shown in Fig. 4.3(c), the u_3 displacement components obtain their local maximum values around the overall displacement peak, with a minimum at the location where the overall displacements are maximum.

Figure 4.6(a) shows the same series of plots as Fig. 4.5(a) for the next time increment (t_2 = 70 min). The color contours display the magnitude of the three-dimensional displacement vector underneath the fibroblast, while the white arrows represent the (u_1, u_2) displacement components. The color bar displays the units in μm, whereas the magnitude of the longest arrow corresponds to 1.8 μm. Figure 4.6(b) plots an enlarged picture of Fig. 4.6(a), highlighting an arbitrarily chosen location to generate a line profile of each displacement component as a function of spatial distance, which is shown in Fig. 4.3(c). The line profiles for both Figs. 4.3(c) and 4.4(c) were chosen at the leading edge of the motile cell. Comparing the contour plots and in particular the line profile plots, Fig. 4.4(c) shows a similar displacement distribution profile. In particular, the u_3 displacement component follows the same trend as in Fig. 4.3(c) attaining two local maxima right before the maximum peak in the total displacement, showing a minimum at the overall displacement peak itself. However, instead of showing only one single total displacement peak, Fig. 4.4(c) depicts two local maxima over an approximate distance of $\sim$ 1 μm.

Figure 4.7 compares the surface displacement fields directly underneath the migrating cells shown in Fig. 4.1(a) and 4.1(b) by highlighting the contribution of the u_3 displacement component. Figures 4.7(a) and 4.7(c) show the displacement contours of the magnitude of the three-dimensional displacement vector whereas Figs. 4.7(b) and 4.7(d) display the magnitude of only the two-dimensional (u_1, u_2) displacement vectors. Side-by-side comparison reveals that most of the deformation occurs in-plane, i.e. (u_1, u_2) are dominating, however there are particular areas where the u_3 displacement component proves to be significant. These areas are found along the periphery of the maximum

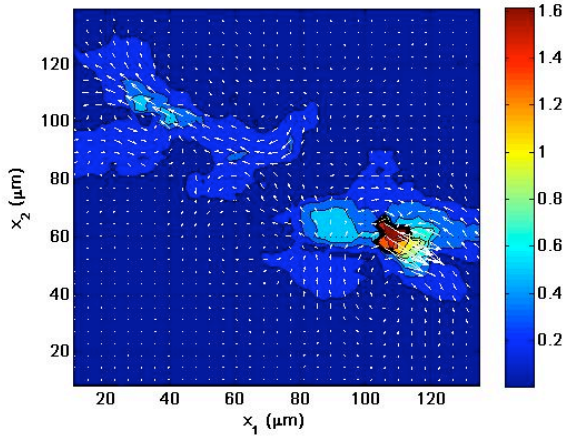

(a) Surface displacement contour plot underneath the migrating cell at $t_1 = 35$ min

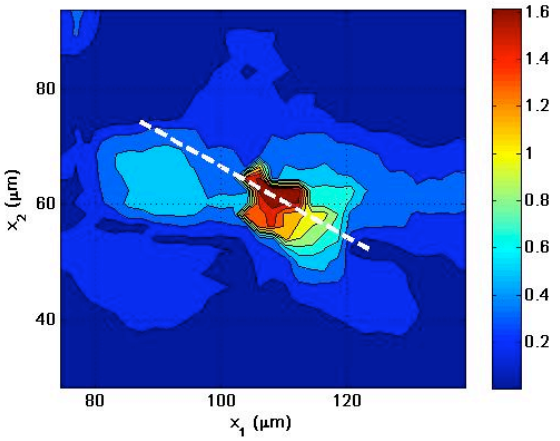

(b) Enlarged view of the contour plot in 4.5(a) and location of displacement line plot shown in 4.5(c) (dashed line)

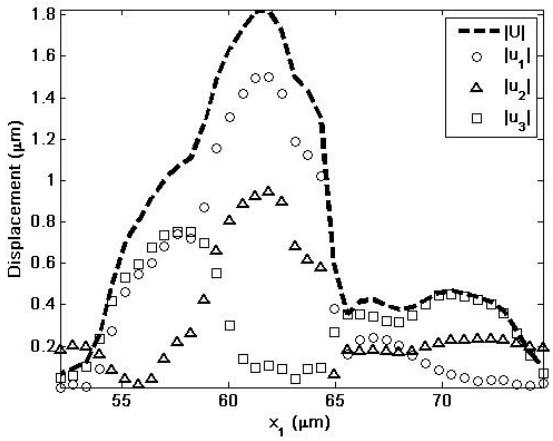

(c) Surface displacement profile along the selected line in 4.5(b)

Figure 4.5: Surface displacement contour and line plot profiles along a particular line in the $x_1 - x_2$ surface plane at $t_1 = 35$ min. Figure 4.5(a) shows the same displacement contours as shown in Fig. 4.1(a), where the color bar represents the magnitude of the three-dimensional displacement vectors in μm, and the white arrows show the direction of the in-plane (u_1,u_2) displacement components only. Figure 4.5(b) shows the zoom-in image of Fig. 4.5(a) highlighting the particular region where the line plot was generated. Figure 4.5(c) illustrates the distribution of all three displacement components along the selected line.

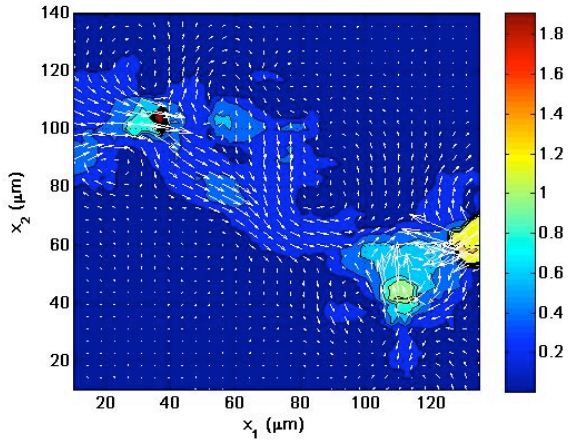

(a) Surface displacement contour plot underneath the migrating cell at $t_2 = 70$ min

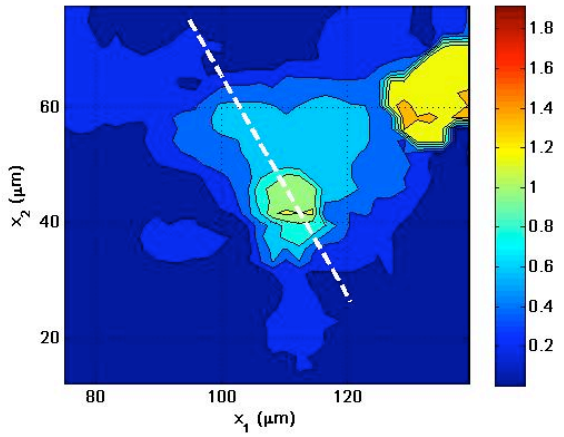

(b) Enlarged view of the contour plot in 4.6(a) and location of displacement line plot shown in 4.6(c) (dashed line)

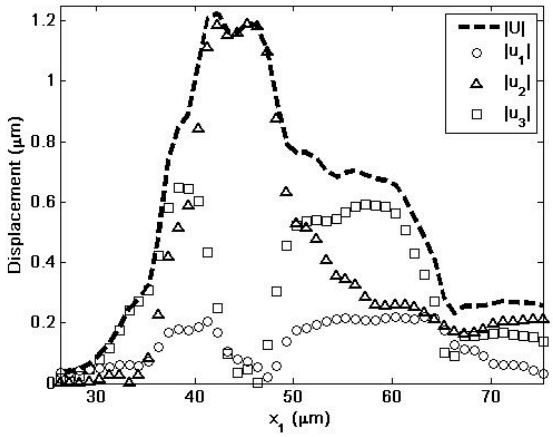

(c) Surface displacement profile along the selected line in 4.6(b)

Figure 4.6: Surface displacement contour and line plot profiles along a particular line in the $x_1 - x_2$ surface plane at $t_2 = 70$ min. Figure 4.6(a) shows the same displacement contours as shown in Fig. 4.1(b), where the color bar represents the magnitude of the three-dimensional displacement vectors in μm, and the white arrows show the direction of the in-plane (u_1,u_2) displacement components only. Figure 4.5(b) shows the zoom-in image of Fig. 4.6(a) highlighting the particular region where the line plot was generated. Figure 4.6(c) illustrates the distribution of all three displacement components along the selected line.

displacement peaks, and are also observed in Figs. 4.5(c) and 4.6(c).

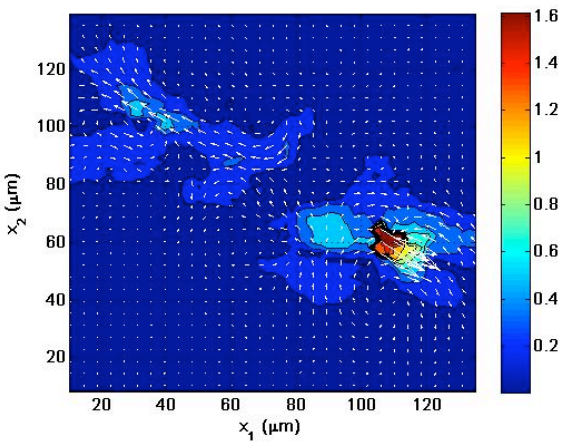

(a) Cell-induced surface displacements (3D) at $t_1 = 35$ min

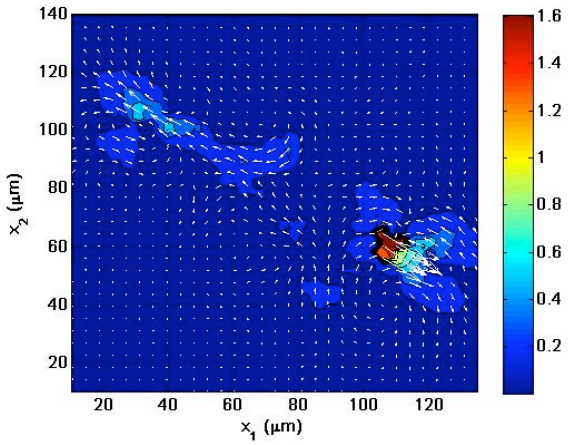

(b) Cell-induced surface displacements (2D) at $t_1 = 35$ min

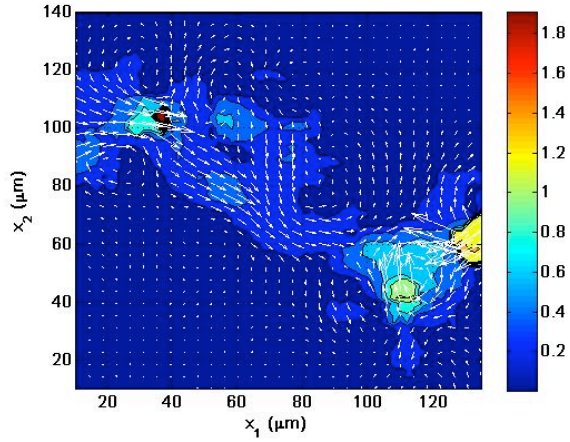

(c) Cell-induced surface displacements (3D) at $t_2 = 70$ min

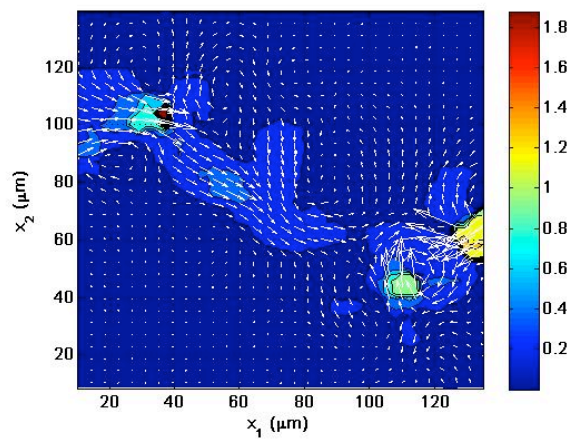

(d) Cell-induced surface displacements (2D) at $t_2 = 70$ min

Figure 4.7: Comparison between the displacement magnitude of all three-dimensional vector components (4.7(a) and 4.7(c)) and the magnitude of the two-dimensional vector components only (4.7(b) and 4.7(d)). The color bar is displaying all displacement values μm, and and the white arrows show the direction of the in-plane (u_1,u_2) displacement components only.

4.3 Three-Dimensional Tractions During Cell Migration on Soft Substrates

This section presents the tractions calculated based upon the measured displacement fields reported in the previous section. Since the determination of the tractions involves calculating the strain tensor and the experimental determination of material constants, the sensitivity of the LSCM-DVC technique in terms of the calculated tractions needs to be assessed. This is accomplished by performing experiments using the same materials setup as in the case for the migrating fibroblasts, but without any cells present. Hence, the measured displacements and calculated tractions are solely due to thermal fluctuations, instrumental and measurement error, and thus establish the sensitivity of the traction calculations. Using standard error analysis the technique can accurately detect stresses and tractions that are greater than 8 Pa or 8 pN/μm^2. All of the subsequently presented Figs. are from the same data set as the displacement results reported in Section 4.2.

Figure 4.8 shows a time evolution of the cell surface tractions during migration over a time span of 140 min. The color contour plots display the magnitude of the three-dimensional traction vector in $pN/\mu m^2$. Again, the linear dimension of the cell in all of the plots is approximately 100 μm. The direction of cell migration is from the left to the right. The localized nature of the tractions is clearly visible in all time frames. As explained earlier due to the degradation of the actin-fluorescent cell stain (GFP-actin), the cell's outline is not always visible directly above some of the stress concentration locations, although the cell is still transmitting force there, as has been confirmed through multiple experiments where GFP-actin was clearly visible.

Figure 4.9 shows the time evolution of the traction field along an arbitrary slice beneath the migration cell's long axis over a time span of 140 min. The tractions acting along the shown plane were calculated through the Cauchy relationship (see Section 4.1.2) with the stress tensor, where the plane is defined by its normal, $\mathbf{n} = (n_1 \quad n_2 \quad 0)^T$, where n_1 and n_2 can be expressed in terms of sine and cosine of the in-plane angle that defines each arbitrarily chosen plane. The decay of the magnitude of the three-dimensional traction vector is shown for the same time series as in figure

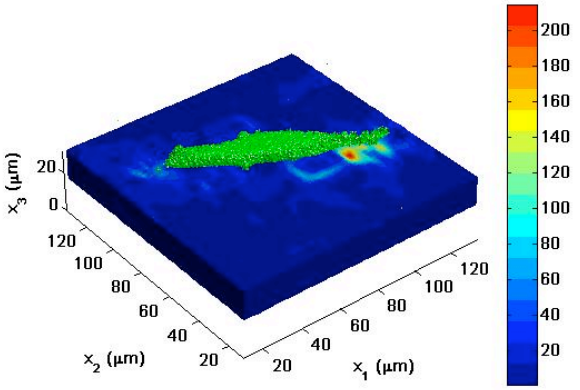

(a) Cell-induced surface tractions at $t_1 = 35$ min

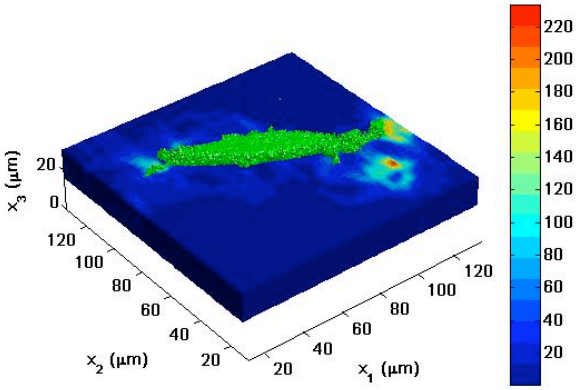

(b) Cell-induced surface tractions at $t_2 = 70$ min

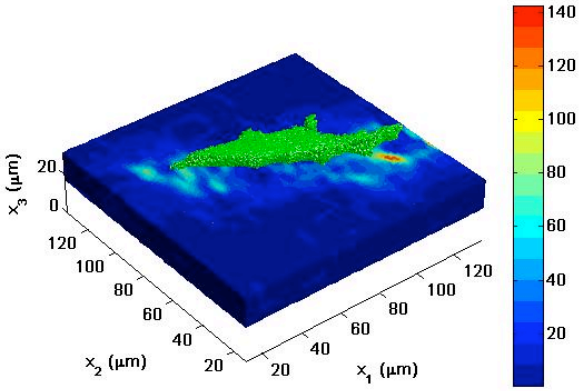

(c) Cell-induced surface tractions at $t_3 = 105$ min

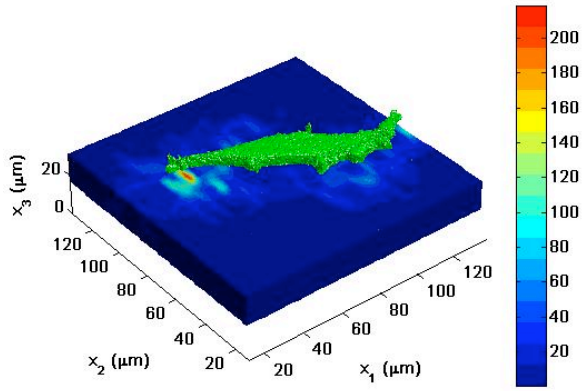

(d) Cell-induced surface tractions at $t_4 = 140$ min

Figure 4.8: Surface contour plots of the magnitude of the three-dimensional traction vector during cell migration. The color bar represents the magnitude of the total three-dimensional surface traction vectors in $pN/\mu m^2$, and the cell (green) is superimposed on the three-dimensional contour plots to show its position with respect to the traction field.

4.8. The color contour plots display the magnitude of the three-dimensional traction vector in $pN/\mu m^2$. The traction contour slices highlight the dynamic interaction of the cell with its substrate characterized by changes in magnitudes and location of the observed tractions. It should be noted that in figure 4.9(d) the cell outline extends past the rear end of the stress concentration (around $x_1 = 30\ \mu m$, $x_2 = 120\ \mu m$).

Figure 4.10 shows the traction field of the arbitrary planar slice shown in Fig. 4.9(a) in more detail. Figure 4.10(a) shows the magnitude of the three-dimensional traction vector as color contours along the same planar slice, while the white arrows represent the (T_3, T_1) traction vector components. The color bar displays the units in $pN/\mu m^2$, whereas the magnitude of the longest arrow corresponds to 40 $pN/\mu m^2$. Figure 4.10(b) plots an enlarged picture of Fig. 4.10(a) highlighting an arbitrarily chosen location to generate a line profile of each traction component as a function of depth (x_3), which is shown in Fig. 4.10(c). Comparing the decay of the magnitude of the three-dimensional traction vector to the decay of the total displacement vector in Fig. 4.3(c), the tractions decay noticeably faster than the corresponding displacements.

Figure 4.11 displays the distribution of the tractions along the same arbitrary plane as in Fig. 4.10 for the next time increment $t_2 = 70$ min. Figure 4.11(a) shows the magnitude of the three-dimensional traction vectors as color contours along the same planar slice, while the white arrows represent the (T_3, T_1) displacement components. The color bar displays the units in $pN/\mu m^2$, whereas the magnitude of the longest arrow corresponds to 100 $pN/\mu m^2$. Figure 4.11(b) plots an enlarged picture of Fig. 4.11(a), highlighting an arbitrarily chosen location to generate a line profile of each traction component as a function of depth (x_3), which is shown in Fig. 4.11(c). The traction contours and line profiles show a similar decay with thickness as presented in Fig. 4.10 at time t_1, however, in Fig. 4.11(c) T_3 is the dominant force term as compared to Fig. 4.10(c) where the in-plane tractions are most significant.

Figures 4.12(a) and 4.13(a) display the surface traction fields presented in Figs. 4.8(a) and 4.8(b) in more detail. In particular, Fig. 4.5(a) shows the magnitude of the three-dimensional traction vectors as color contours directly underneath the migrating cell, while the white arrows

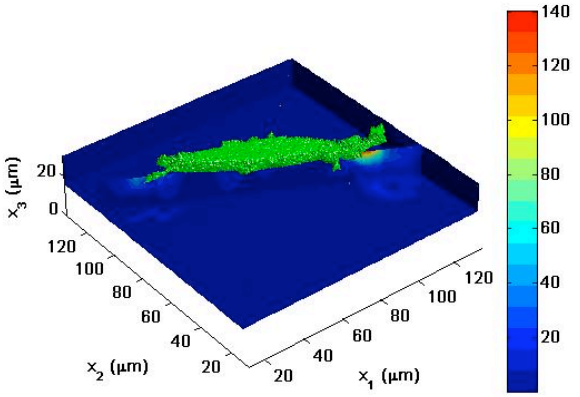

(a) Cell tractions at $t_1 = 35$ min

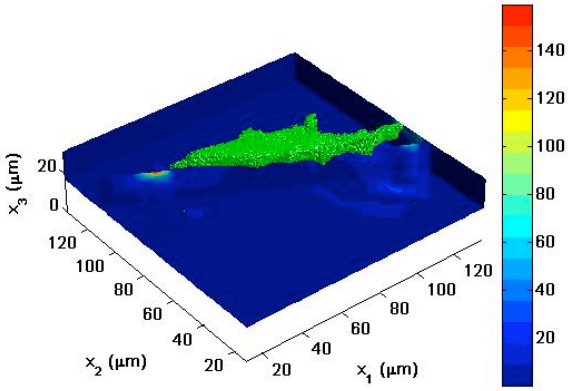

(b) Cell tractions at $t_2 = 70$ min

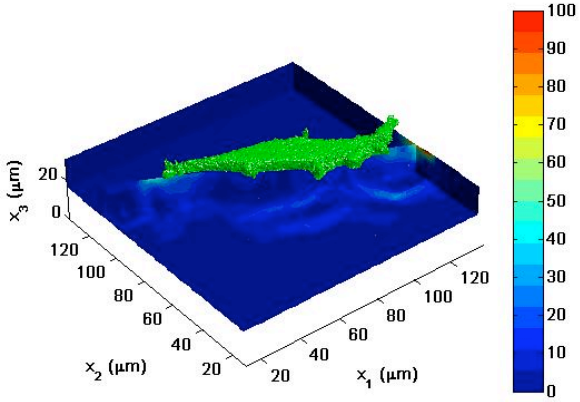

(c) Cell tractions at $t_3 = 105$ min

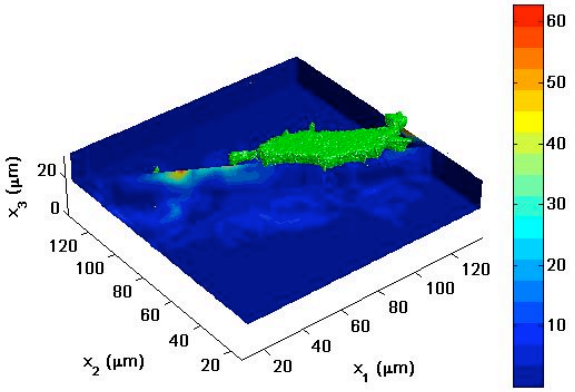

(d) Cell tractions at $t_4 = 140$ min

Figure 4.9: Arbitrary traction contour slices along the long axis of the cell. The color bar indicates the magnitude of the three-dimensional traction vectors along that particular plane in units of $pN/\mu m^2$. The slices of the traction contours underneath the migrating cells correspond to the displacement slices shown in Fig. 4.2. The two edges in the image are included to show that there are negligible tractions detected from neighboring cells (contours are dark blue). The cell (green) is superimposed on the three-dimensional contour plots to show its position with respect to the traction field.

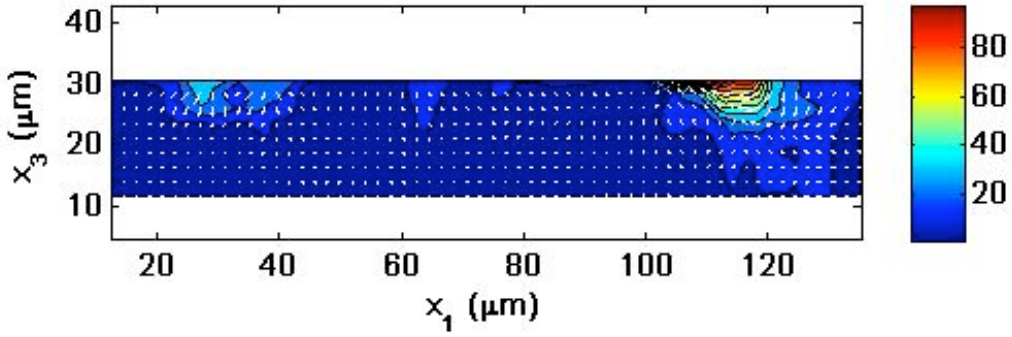

(a) Cross-sectional traction contour plot through the substrate thickness at $t_1 = 35$ min

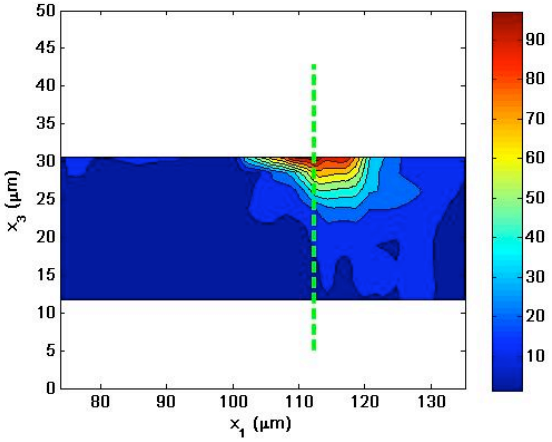

(b) Enlarged view of the contour plot in 4.10(a) and the location of traction line plot shown in 4.10(c)

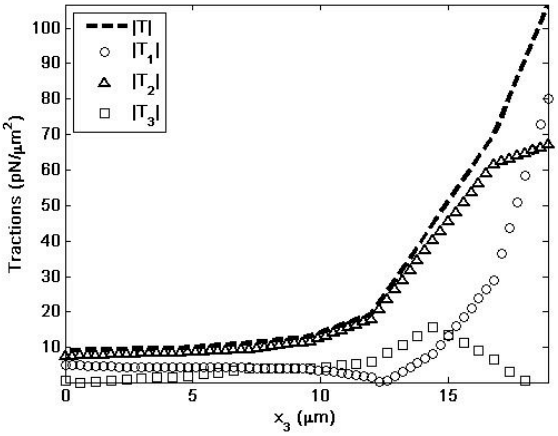

(c) Traction force line profile through the thickness of the gel (x_3). The maximum x_3 value corresponds to the gel surface

Figure 4.10: Traction contour and line plot profiles as a function of depth (x_3) through the thickness of the gel at time $t_1 = 35$ min. Figure 4.10(a) shows the same traction contours along the long axis of the cell as shown in Fig. 4.9(a), where the color bar represents the magnitude of the three-dimensional traction vectors along that particular plane, and the white arrows show the direction of the in-plane (T_1,T_3) traction components only. Figure 4.10(b) shows the zoom-in image of Fig. 4.10(a), whereas Fig. 4.10(c) illustrates the decay of all traction components and the magnitude of the three-dimensional traction vector in the x_3 direction. The color bar units are displayed in $pN/\mu m^2$.

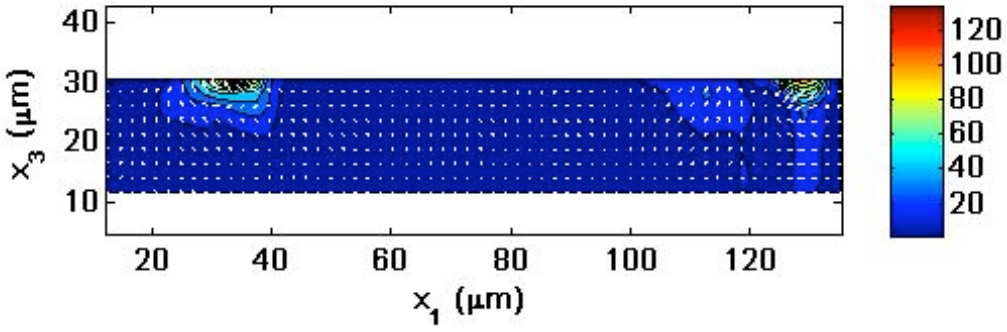

(a) Cross-sectional traction contour plot through the substrate thickness at $t_1 = 70$ min

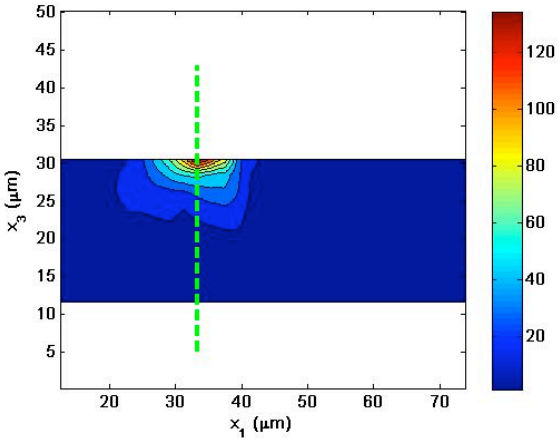

(b) Enlarged view of the contour plot in 4.11(a) and location of the traction line plot shown in 4.11(c)

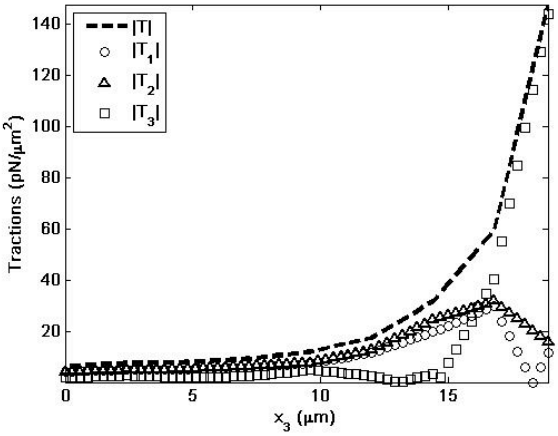

(c) Traction line profile through the thickness of the gel (x_3). The maximum x_3 value corresponds to the gel surface.

Figure 4.11: Traction contour and line plot profiles as a function of depth (x_3) through the thickness of the gel at time $t_2 = 70$ min. Figure 4.11(a) shows the same traction contours along the long axis of the cell as shown in Fig. 4.9(b), where the color bar represents the magnitude of the three-dimensional traction vectors along that particular plane, and the white arrows show the direction of the in-plane (T_1,T_3) traction components only. Figure 4.11(b) shows the zoom-in image of Fig. 4.11(a), whereas Fig. 4.11(c) illustrates the decay of all traction components and the magnitude of the three-dimensional traction vector in the x_3 direction. The color bar units are displayed in $pN/\mu m^2$.

represent the (T_1, T_2) traction components. The color bar displays the units in $pN/\mu m^2$, whereas the magnitude of the longest arrow corresponds to 140 $pN/\mu m^2$. Figure 4.12(b) plots an enlarged picture of Fig. 4.12(a), highlighting an arbitrarily chosen location to generate a line profile of each traction component as a function of spatial distance, which is shown in Fig. 4.12(c). Here, the tractions follow an almost Gaussian distribution obtaining a maximum value of 172 $pN/\mu m^2$ over a length of $\sim$ 1 μm, most likely corresponding to the particular location of a focal adhesion complex.

Figure 4.13(a) shows the same series of plots as Fig. 4.12(a) for the next time increment (t_2 = 70 min). The color contours display the magnitude of the three-dimensional traction vectors underneath the fibroblast, while the white arrows represent the (T_1, T_2) traction components. The color bar displays the units in $pN/\mu m^2$, whereas the magnitude of the longest arrow corresponds to 140 $pN/\mu m^2$. Figure 4.13(b) plots an enlarged picture of Fig. 4.13(a), highlighting an arbitrarily chosen location to generate a line profile of each traction component (T_1, T_2, T_3) and the magnitude of the three-dimensional traction vector ($|\mathbf{T}|$) as a function of spatial distance, which is shown in Fig. 4.3(c). The line profiles in Figs. 4.3(c) and 4.13(c) were chosen at the leading edge of the motile cell. Comparing the contour plots and in particular the two line profile plots, Fig. 4.13(c) shows a broader traction profile with two local maxima. The T_1 traction component attains a single maximum coinciding with the maximum peak of the total traction vector. The T_2 traction component obtains two smaller single peaks at the same spatial location as the overall traction vector, while the T_3 traction component reaches its highest value close to the location where the local minimum value of the total traction vector is shown.

Figure 4.14 compares the surface traction fields directly underneath the migrating cells shown in Figs. 4.8(a) and 4.8(b) by highlighting the contribution of the T_3 traction component. Figures 4.14(a) and 4.14(c) show surface contours of the magnitude of the three-dimensional traction vectors whereas Figs. 4.14(b) and 4.14(d) display the magnitude of only the two-dimensional, in-plane (T_1, T_2) traction vectors. Side-by-side comparison reveals that the cell applies mostly shear tractions (T_1, T_2). While the contribution of T_3 is observed in a few areas, shown in Figs. 4.12(c) and 4.13(c), its overall contribution is relatively insignificant for the given time increments t_1 and t_2.

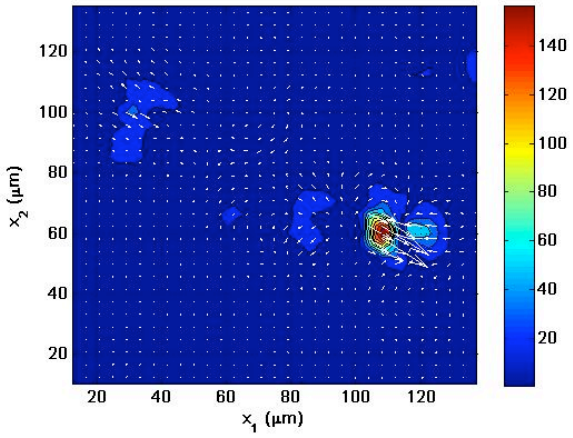

(a) Surface tractions contour plot underneath the migrating cell at $t_1 = 35$ min

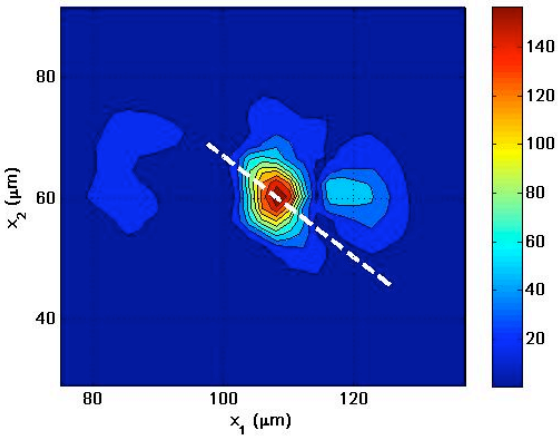

(b) Enlarged view of the contour plot in 4.12(a) and location of the traction line plot shown in 4.12(c)

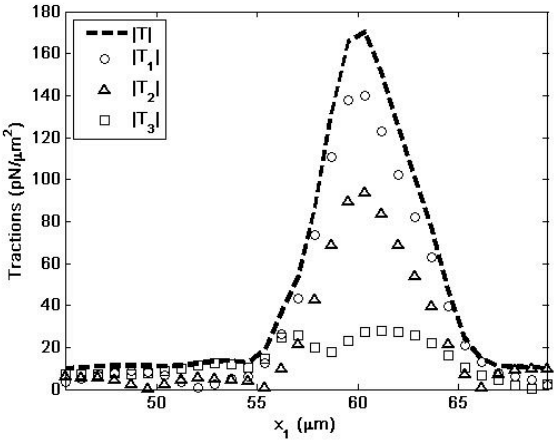

(c) Traction force profile along the selected line in 4.12(b)

Figure 4.12: Surface tractions contour and line plot profiles along a particular line in the $x_1 - x_2$ top surface plane at $t_1 = 35$ min. Figure 4.12(a) shows the same traction contours as shown in Fig. 4.8(a), where the color bar represents the magnitude of the three-dimensional surface traction vectors and the white arrows show the direction of the in-plane (T_1,T_2) traction components only. The color bar units are in $pN/\mu m^2$. Figure 4.5(b) shows the zoom-in image of Fig. 4.12(a) highlighting the particular region, where the line plot was generated. Figure 4.12(c) illustrates the distribution of all three traction components and the magnitude of the three-dimensional traction vector along the drawn line.

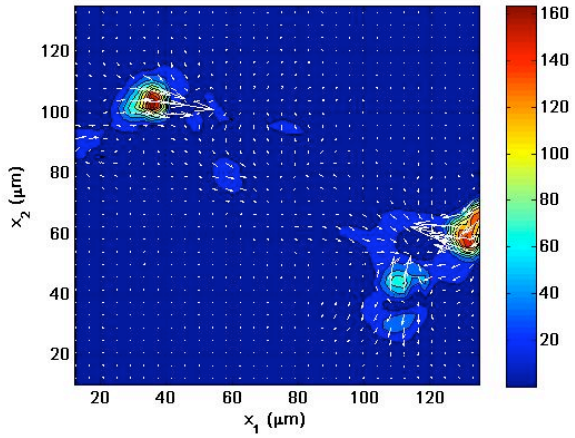

(a) Surface tractions contour plot underneath the migrating cell at $t_2 = 70$ min

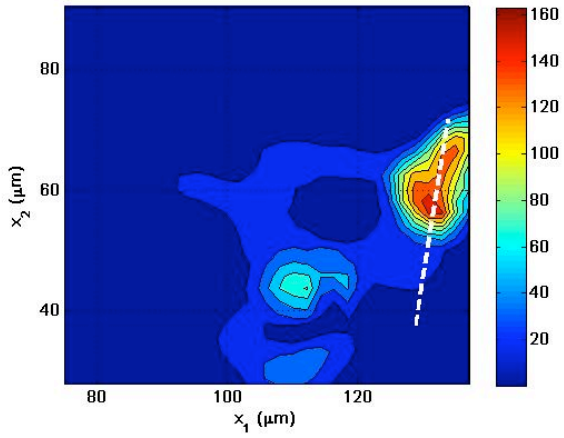

(b) Enlarged view of the contour plot in 4.13(a) and location of the traction line plot shown in 4.13(c)

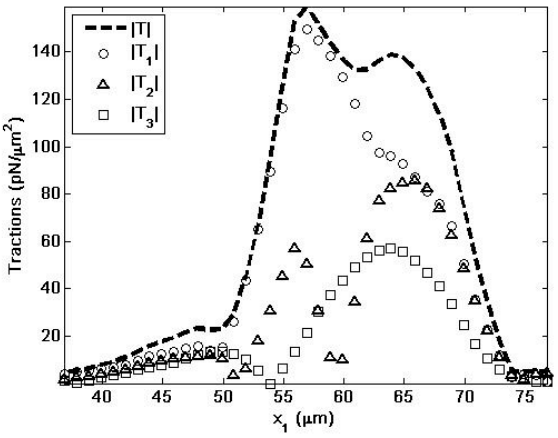

(c) Traction force profile along the selected line in 4.13(b)

Figure 4.13: Surface traction contour and line plot profiles along a particular line in the $x_1 - x_2$ top surface plane at $t_2 = 70$ min. Figure 4.13(a) shows the same traction force contours as shown in Fig. 4.8(b), where the color bar represents the magnitude of the three-dimensional surface traction vectors and the white arrows show the direction of the in-plane (T_1,T_2) traction components only. The color bar units are $pN/\mu m^2$. Figure 4.6(b) shows the zoom-in image of Fig. 4.13(a) highlighting the particular region, where the line plot was generated. Figure 4.13(c) illustrates the distribution of all three traction components and the magnitude of the three-dimensional traction vector along the drawn line.

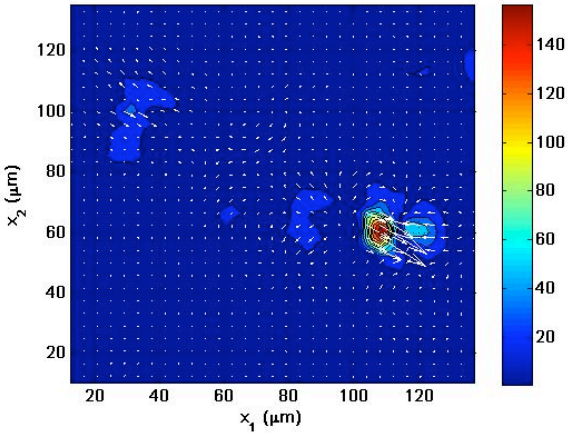

(a) Cell-induced surface tractions (3D) at $t_1 = 35$ min

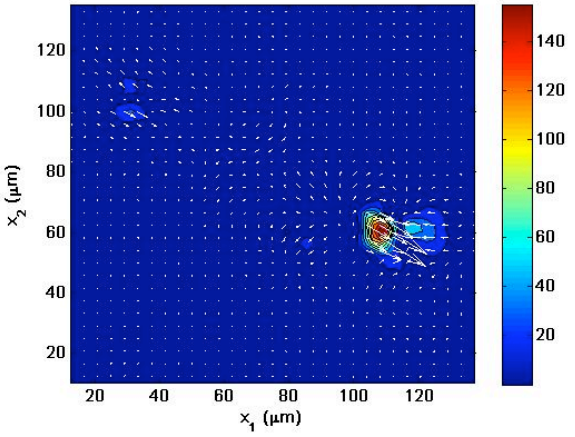

(b) Cell-induced surface tractions (2D) at $t_1 = 35$ min

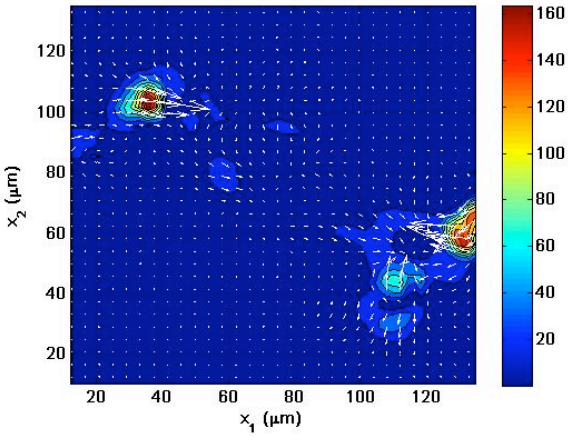

(c) Cell-induced surface tractions (3D) at $t_2 = 70$ min

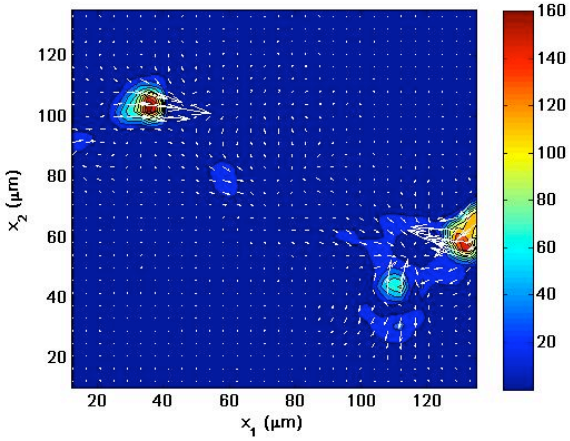

(d) Cell-induced surface tractions (2D) at $t_2 = 70$ min

Figure 4.14: Comparison between the magnitude of the three-dimensional traction vector (4.14(a) and 4.14(c)) and the magnitude of the two-dimensional traction vector (T_1, T_2) components only (4.14(b) and 4.14(d))). The color bar is displaying all traction values in $pN/\mu m^2$, and and the white arrows show the direction of the in-plane (T_1,T_2) traction components only.

4.4 Three-Dimensional Displacements During Cell Migration on Stiff Substrates

This section presents the full-field three-dimensional displacements induced by migration cells on *stiff* substrates (for definitions of *soft* and *stiff* refer to beginning of Chapter 4). All Figs. and results are displayed in the same format as in the previous sections. One observation worth mentioning is that the magnitude of the measured displacement fields are of the same order as those for the *soft* substrates and thus appear independent of the Young's modulus of the substrate material over the range of moduli investigated. These findings are discussed in more detail in Section 4.7.

Figure 4.15 shows a time evolution of the surface displacement fields beneath a migration cell over a time span of 140 min. The color contour plots display the magnitude of the three-dimensional displacement vector in μm. The linear dimension of the cell in all of the plots is approximately 80 - 100 μm. The direction of cell migration is from the left to right. The cell migration speed, as determined by tracking the nucleus of the cell, is ≈ 8 μm/hr.

Figure 4.16 shows the time evolution of the displacement field along an arbitrary slice beneath the migration cell's long axis over a time span of 140 min. Here the decay of the magnitude of the three-dimensional displacement vectors are shown for the same time series as in Fig. 4.15. The color contour plots display the magnitude of the three-dimensional displacement vector in μm. The displacement contour slices highlight the dynamic interaction of the cell with its substrate characterized by changes in magnitudes and location of the observed displacements.

Figure 4.17 shows the displacement field of the arbitrary planar slice in Fig. 4.16(a) in more detail. Figure 4.17(a) shows the magnitude of the three-dimensional displacement vector as color contours along the same planar slice, while the white arrows represent the (u_3, u_1) displacement components. The color bar displays the units in μm, whereas the magnitude of the longest arrow corresponds to 1 μm. Figure 4.17(b) plots an enlarged picture of Fig. 4.17(a), highlighting an arbitrarily chosen location to generate a line profile of each displacement component as a function of depth (x_3), which is shown in Fig. 4.17(c). While the overall displacement magnitude

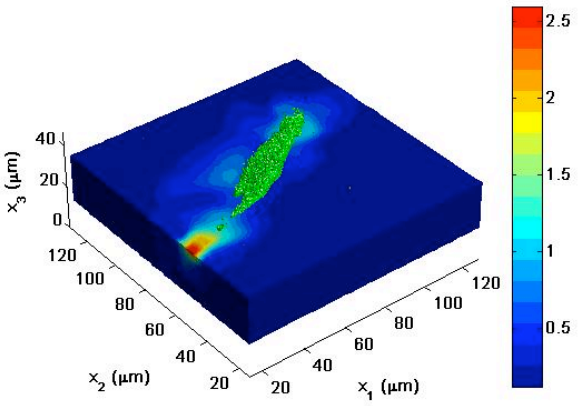

(a) Cell-induced surface displacements at $t_1 = 35$ min

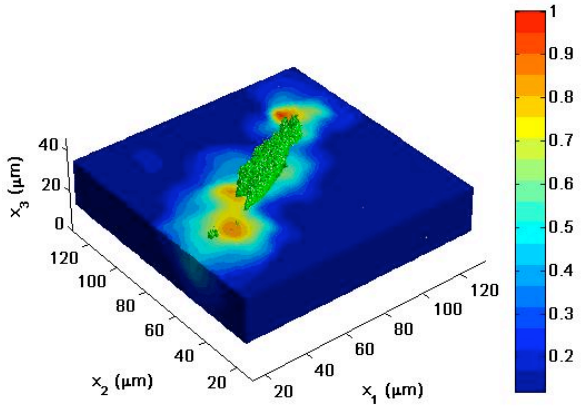

(b) Cell-induced surface displacements at $t_2 = 70$ min

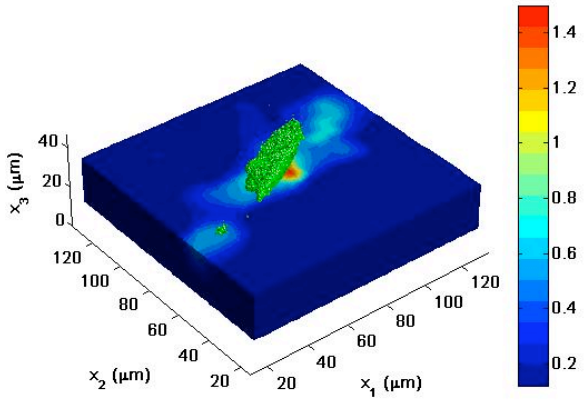

(c) Cell-induced surface displacements at $t_3 = 105$ min

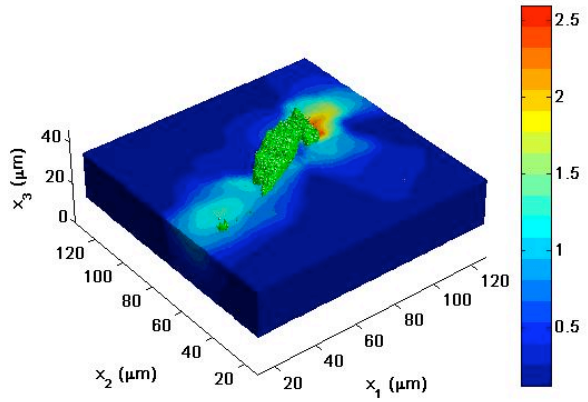

(d) Cell-induced surface displacements at $t_4 = 140$ min

Figure 4.15: Surface contour plots of the magnitude of the three-dimensional displacment vector during cell migration. The color bar represents the magnitude of the total three-dimensional displacement vectors in μm, and the cell (green) is superimposed on the three-dimensional contour plots to show its position with respect to the deformation field.

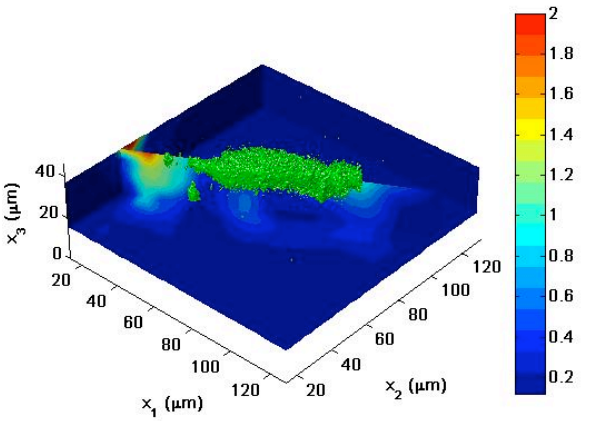

(a) Cell-induced displacements at $t_1 = 35$ min

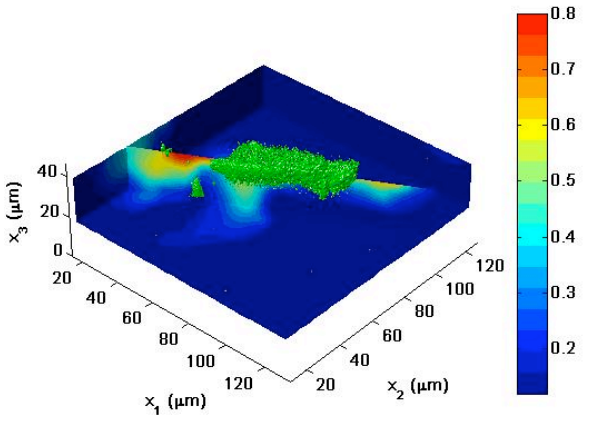

(b) Cell-induced displacements at $t_2 = 70$ min

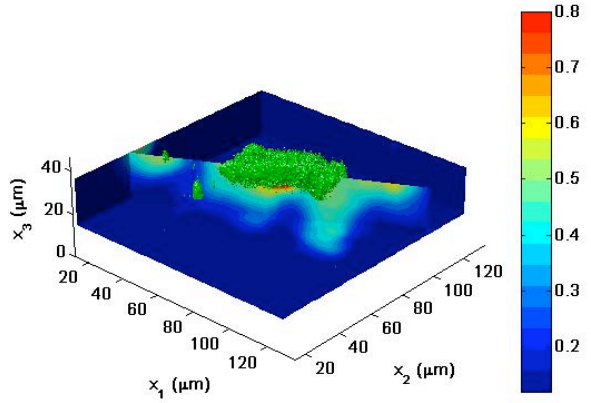

(c) Cell-induced displacements at $t_3 = 105$ min

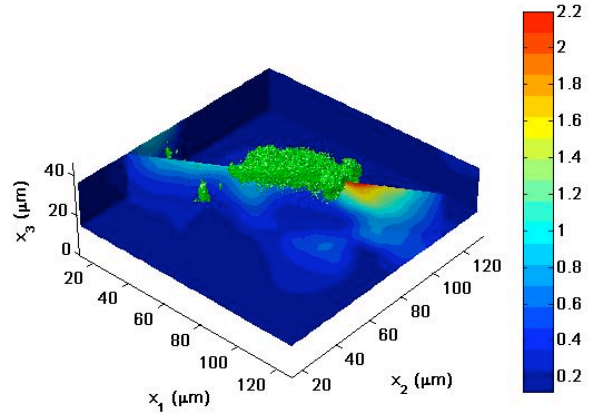

(d) Cell-induced displacements at $t_4 = 140$ min

Figure 4.16: Arbitrary displacement contour slices along the long axis of the cell. The slices of displacement contours underneath migrating cells show significant deformation in the normal plane that decay along the thickness of the sample. The two edges in the image are included to show that there are negligible displacements detected from neighboring cells (contours are dark blue). The color bar represents the magnitude of the total three-dimensional displacement vectors in μm, and the cell (green) is superimposed on the three-dimensional contour plots to show its position with respect to the deformation field.

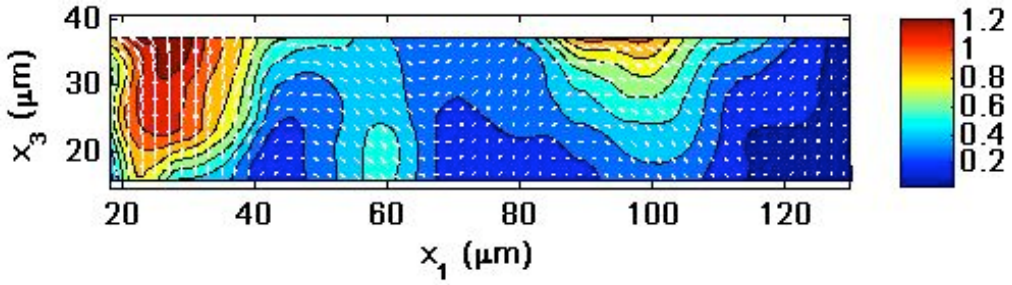

(a) Cross-sectional displacement contour plot through the substrate thickness at $t_1 = 35$ min

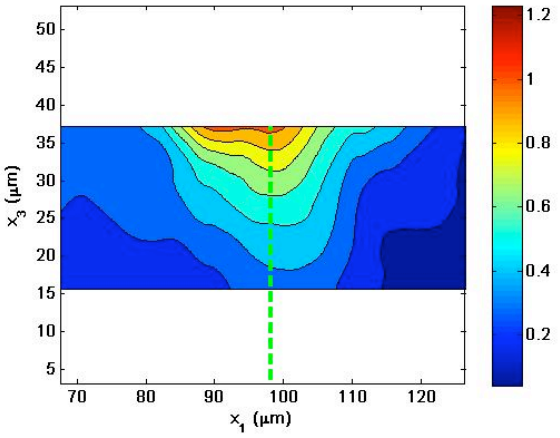

(b) Enlarged view of the contour plot in 4.17(a) and location of displacement line plot shown in 4.17(c)

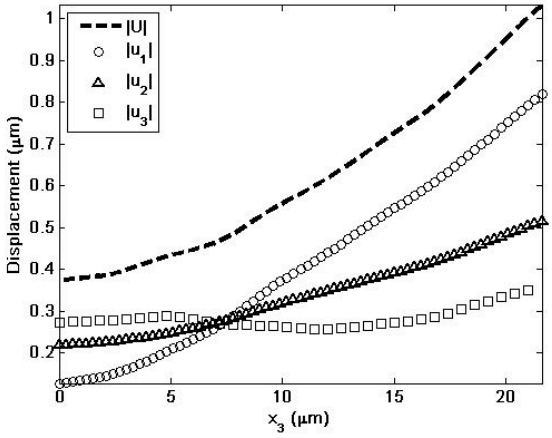

(c) Displacement line profile through the thickness of the gel (x_3). The maximum x_3 value corresponds to the gel surface.

Figure 4.17: Displacement contour and line plot profiles as a function of depth (x_3) through the thickness of the gel. Figure 4.17(a) shows the same displacement contours along the long axis of the cell as shown in Fig. 4.16(a), where the color bar represents the magnitude of the three-dimensional displacement vectors in μm, and the white arrows show the direction of the in-plane (u_1,u_3) displacement components only. Figure 4.17(b) shows the zoom-in image of Fig. 4.17(a), whereas Fig. 4.17(c) illustrates the decay of all three displacement components and the magnitude of the three-dimensional displacement vector in the x_3 direction.

decays approximately as $x_3^{3/2}$, the magnitude of the individual displacement components highlights the importance of the u_3 component at that particular time increment (t_1). Figure 4.18 displays the displacement distribution along the same arbitrary plane as in Fig. 4.17 for the next time increment $t_2 = 70$ min. Figure 4.18(a) shows the magnitude of the three-dimensional displacement vector as color contours along the same planar slice, while the white arrows represent the (u_3, u_1) displacement components. The color bar displays the units in μm, whereas the magnitude of the longest arrow corresponds to 0.6 μm. Figure 4.17(b) plots an enlarged picture of Fig. 4.17(a), highlighting an arbitrarily chosen location to generate a line profile of each displacement component as a function of depth (x_3), which is shown in Fig. 4.17(c). The displacement contour and line profiles show a similar decay with thickness than presented in Fig. 4.17 at time t_1.

Figures 4.19 and 4.20 display the surface displacement fields presented in Figs. 4.15(a) and 4.15(b) in more detail. In particular, Fig. 4.19(a) shows the magnitude of the three-dimensional displacement vector as color contours directly underneath the migrating cell, while the white arrows represent the (u_1, u_2) displacement components. The color bar displays the units in μm, whereas the magnitude of the longest arrow corresponds to 1.4 μm. Figure 4.19(b) plots an enlarged picture of Fig. 4.19(a), highlighting an arbitrarily chosen location to generate a line profile of each displacement component as a function of spatial distance, which is shown in Fig. 4.17(c). The displacement distribution is primarily dominated by the in-plane displacements with the u_3 displacement component showing its highest values at the periphery of the line profile. This particular displacement trend for the u_3 component is also observed in the *softer* substrate materials (see Fig. 4.5 and 4.6).

Figure 4.20(a) shows the same series of plots as Fig. 4.19(a) for the next time increment ($t_2 =$ 70 min). The color contours display the magnitude of the three-dimensional displacement vector underneath the fibroblast, while the white arrows represent the (u_1, u_2) displacement components. The color bar displays the units in μm, whereas the magnitude of the longest arrow corresponds to 1.8 μm. Figure 4.20(b) plots an enlarged picture of Fig. 4.20(a), highlighting an arbitrarily chosen location to generate a line profile of each displacement component as a function of spatial distance, which is shown in Fig. 4.17(c). The line profiles for both Figs. 4.17(c) and 4.18(c) were chosen at

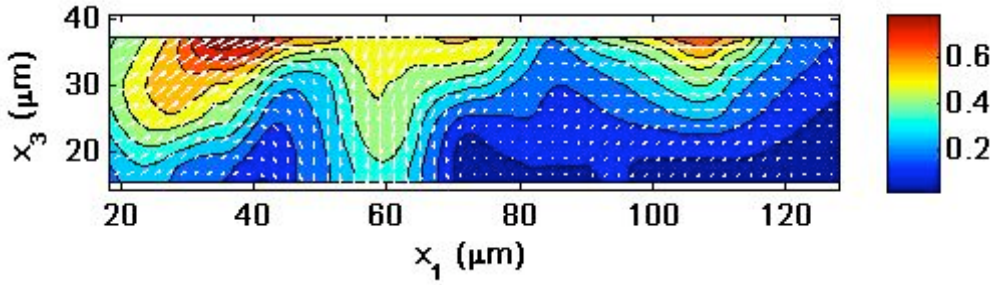

(a) Cross-sectional displacement contour plot through the substrate thickness at $t_2 = 70$ min

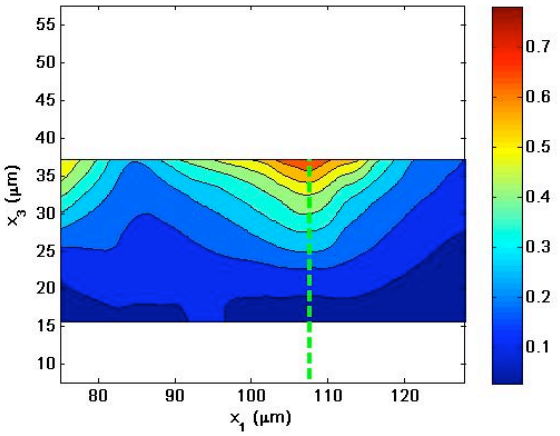

(b) Enlarged view of the contour plot in 4.18(a) and location of displacement line plot shown in 4.18(c)

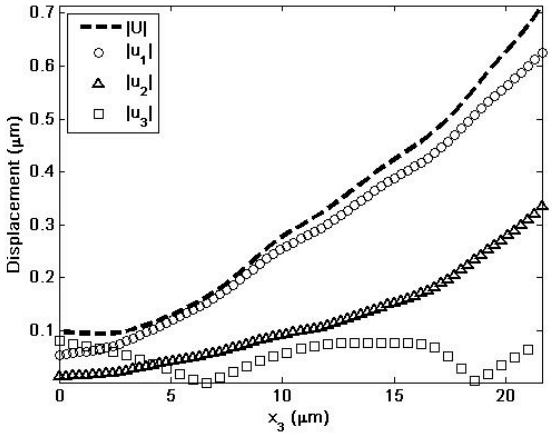

(c) Displacement line profile through the thickness of the gel (x_3). The maximum x_3 value corresponds to the gel surface.

Figure 4.18: Displacement contour and line plot profiles as a function of depth (x_3) through the thickness of the gel. Part 4.18(a) shows the same displacement contours along the long axis of the cell as shown in Fig. 4.16(b), where the color bar represents the magnitude of the three-dimensional displacement vectors in μm, and the white arrows show the direction of the in-plane (u_1,u_3) displacement components only. Figure 4.18(b) shows the zoom-in image of Fig. 4.18(a), whereas Fig. 4.18(c) illustrates the decay of all three displacement components and the magnitude of the three-dimensional displacement vector in the x_3 direction.

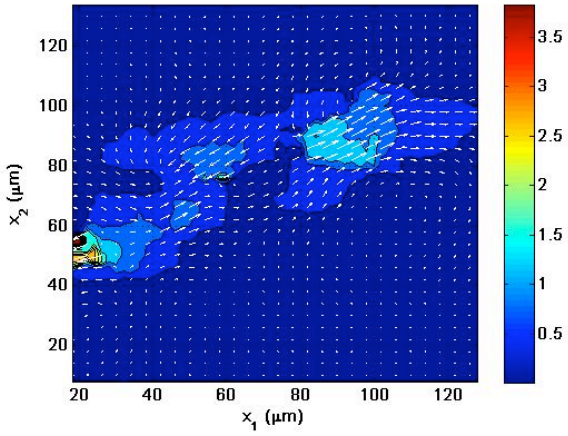

(a) Surface displacement contour plot underneath the migrating cell at $t_1 = 35$ min

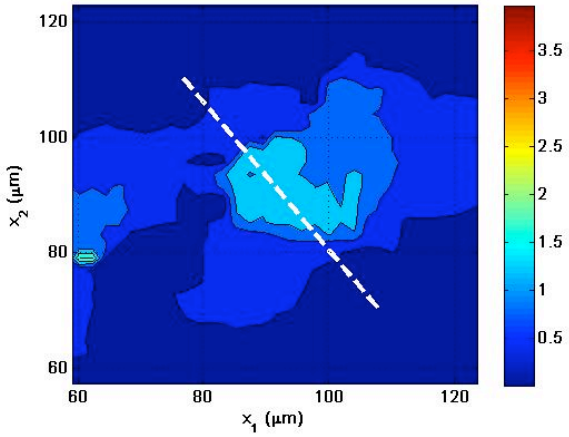

(b) Enlarged view of the contour plot in 4.5(a) and location of displacement line plot shown in 4.19(c)

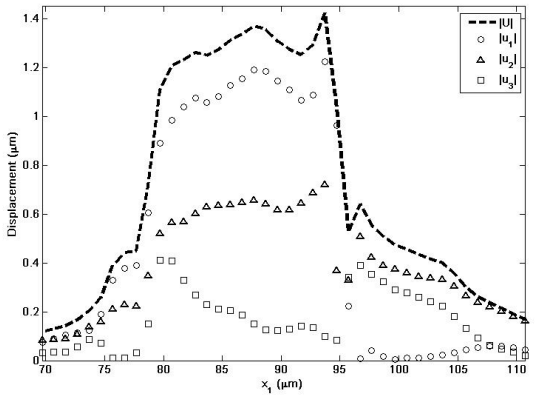

(c) Displacement profile along the selected line in 4.5(b)

Figure 4.19: Surface displacement contour and line plot profiles along a particular line in the $x_1 - x_2$ top surface plane at $t_1 = 35$ min. Figure 4.19(a) shows the same displacement contours as shown in Fig. 4.15(a), where the color bar represents the magnitude of the three-dimensional displacement vectors in μm, and the white arrows show the direction of the in-plane (u_1,u_2) displacement components only. Figure 4.19(b) shows the zoom-in image of Fig. 4.19(a) highlighting the particular region, where the line plot was generated. Figure 4.19(c) illustrates the distribution of all three displacement components and the magnitude of the three-dimensional displacement vector along the drawn line.

the leading edge of the motile cell. Comparing the contour plots and in particular the line profile plots, Fig. 4.18(c) shows a a narrower, Gaussian-like displacement distribution profile as compared to Fig. 4.17(c).

Figure 4.21 compares the surface displacement fields directly underneath the migrating cells shown in Fig. 4.15(a) and 4.15(b) by highlighting the contribution of the u_3 displacement component. Figures 4.21(a) and 4.21(c) show the displacement contours of the magnitude of the three-dimensional displacement vector whereas Figs. 4.21(b) and 4.21(d) display the magnitude of only the two-dimensional (u_1, u_2) displacement vectors. Side-by-side comparison reveals that most of the deformation occurs in-plane (u_1, u_2), however there are particular areas where the u_3 proves to be significant. These areas are found along the periphery of the maximum displacement peaks, which is also observed in Figs. 4.19(c) and 4.20(c).

4.5 Three-Dimensional Tractions During Cell Migration on Stiff Substrates

This section presents the traction calculation based upon the measured displacement field reported in Section 4.4. Following the same error analysis as in Section 4.3 the technique is sensitive to stresses and tractions that are greater than 80 Pa or 80 pN/μm^2. All of the subsequently presented Figs. are from the same data set as the displacement results reported in Section 4.4.

Figure 4.22 shows a time evolution of the cell surface tractions during migration over a time span of 140 min. The color contour plots display the magnitude of the three-dimensional traction vector in $pN/\mu m^2$. Again, the linear dimension of the cell in all of the plots is approximately 80 - 100 μm. The direction of cell migration is from the left to the right. The localized nature of the tractions is clearly visible in all time frames. As described earlier, due to the degradation of the actin-fluorescent cell stain (GFP-actin), the cell's outline is not always visible directly above some of the stress concentration locations, although the cell is still transmitting force there, as has been confirmed through multiple experiments where GFP-actin was clearly visible.

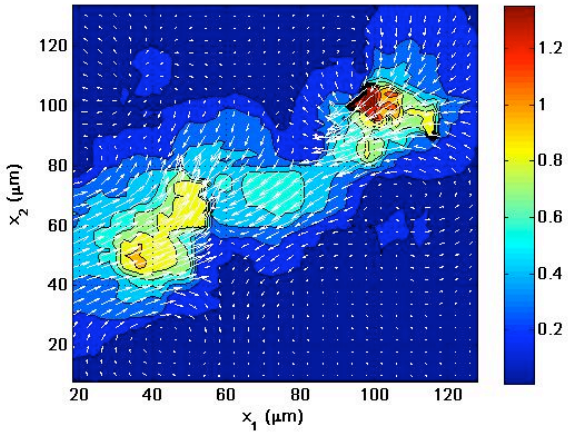

(a) Surface displacement contour plot underneath the migrating cell at $t_2 = 70$ min

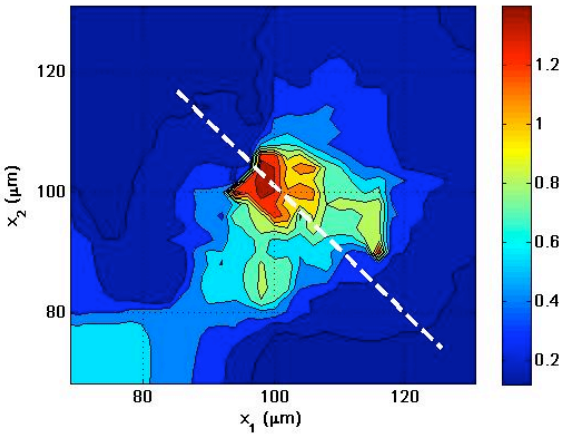

(b) Enlarged view of the contour plot in 4.6(a) and location of displacement line plot shown in 4.20(c)

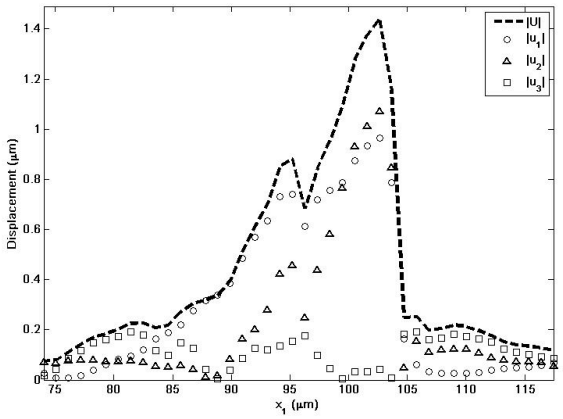

(c) Displacement profile along the selected line in 4.6(b)

Figure 4.20: Surface displacement contour and line plot profiles along a particular line in the $x_1 - x_2$ top surface plane at $t_2 = 70$ min. Figure 4.20(a) shows the same displacement contours as shown in Fig. 4.15(b), where the color bar represents the magnitude of the three-dimensional displacement vectors in μm, and the white arrows show the direction of the in-plane (u_1,u_2) displacement components only. Figure 4.19(b) shows the zoom-in image of Fig. 4.20(a) highlighting the particular region, where the line plot was generated. Figure 4.20(c) illustrates the distribution of all three displacement components and the magnitude of the three-dimensional displacement vector along the drawn line.

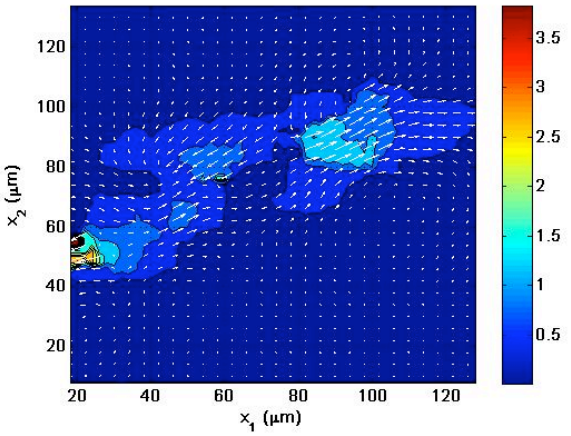

(a) Cell-induced surface displacements (3D) at $t_1 = 35$ min

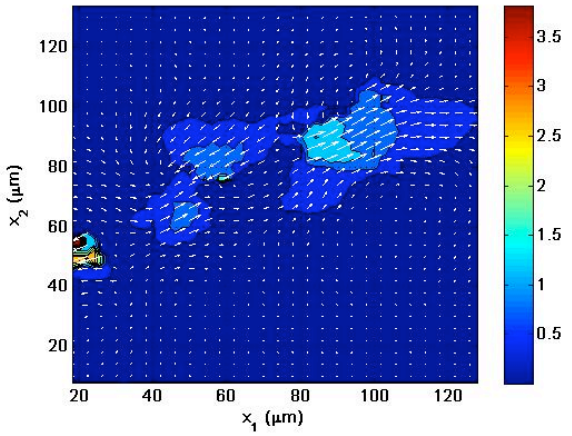

(b) Cell-induced surface displacements (2D) at $t_1 = 35$ min

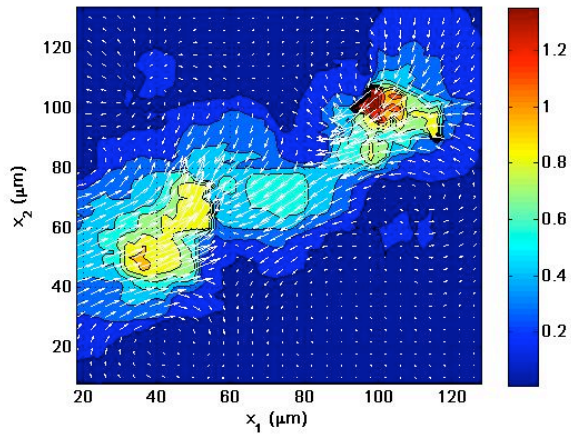

(c) Cell-induced surface displacements (3D) at $t_2 = 70$ min

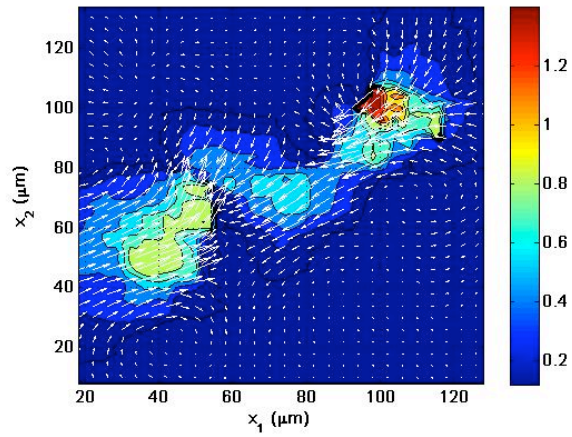

(d) Cell-induced surface displacements (2D) at $t_2 = 70$ min

Figure 4.21: Comparison between the displacement magnitude of all three-dimensional vector components (4.21(a) and 4.21(c)) and the magnitude of the two-dimensional vector components only (4.21(b) and 4.21(d)). The color bar is displaying all displacement values in μm, and and the white arrows show the direction of the in-plane (u_1,u_2) displacement components only.

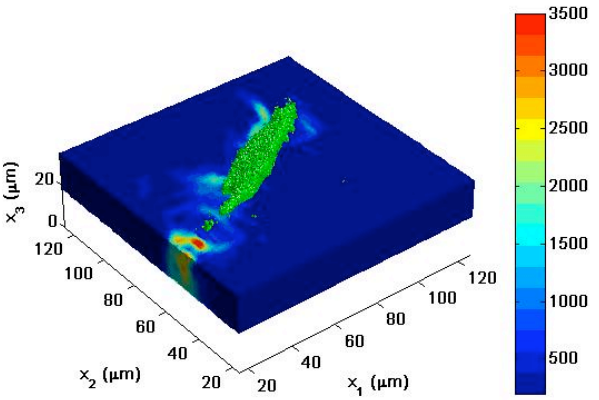

(a) Cell-induced surface tractions at $t_1 = 35$ min

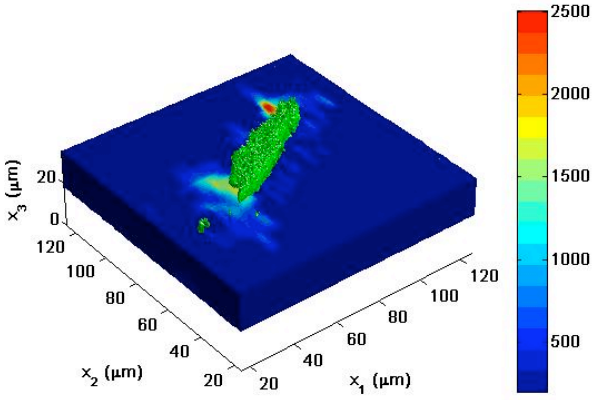

(b) Cell-induced surface tractions at $t_2 = 70$ min

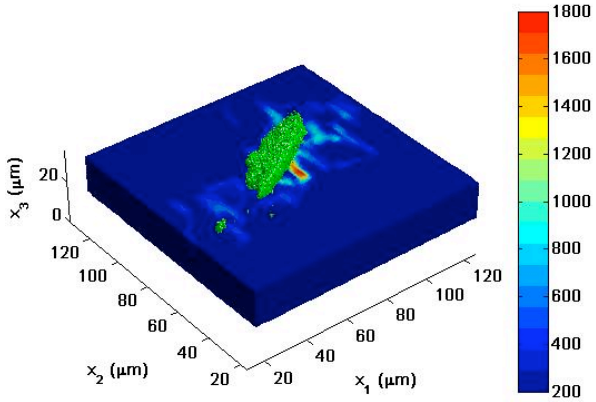

(c) Cell-induced surface tractions at $t_3 = 105$ min

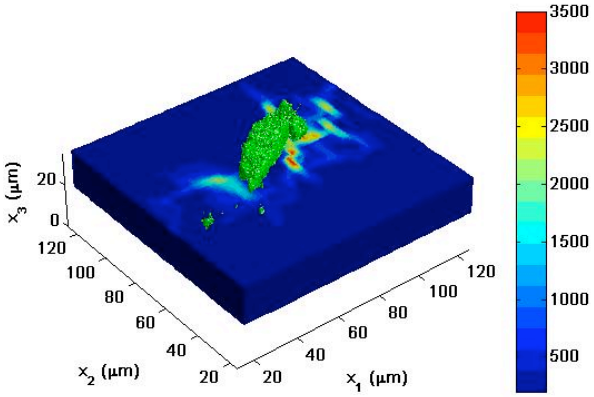

(d) Cell-induced surface tractions at $t_4 = 140$ min

Figure 4.22: Surface contour plots of the magnitude of the three-dimensional traction vector during cell migration. The color bar represents the magnitude of the total three-dimensional surface traction vectors with units in $pN/\mu m^2$, and the cell (green) is superimposed on the three-dimensional contour plots to show its position with respect to the traction field.

Figure 4.23 shows the time evolution of the traction field along an arbitrary slice beneath the migration cell's long axis over a time span of 140 min. The tractions acting along the shown plane were calculated as previously described (see Section 4.3). The decay of the magnitude of the three-dimensional traction vector is shown for the same time series as in Fig. 4.22. The color contour plots display the magnitude of the three-dimensional traction vector in $pN/\mu m^2$. The traction contour slices highlight the dynamic interaction of the cell with its substrate, characterized by changes in magnitudes and location of the observed tractions. It should be noted that in all Figs. the actual cell outline most likely extends further than is shown by the green rendered cell, where the GFP-actin is degraded as explained earlier.

Figure 4.24 examines the traction field of the arbitrary planar slice in Fig. 4.23(a) in more detail. Figure 4.24(a) shows the magnitude of the three-dimensional traction vector as color contours along the same planar slice, while the white arrows represent the (T_3, T_1) traction vector components. The color bar displays the units in $pN/\mu m^2$, whereas the magnitude of the longest arrow corresponds to 3000 $pN/\mu m^2$. Figure 4.24(b) plots an enlarged picture of Fig. 4.10(a), highlighting an arbitrarily chosen location to generate a line profile of each traction component as a function of depth (x_3), which is shown in Fig. 4.24(c). The decay of the total traction vector appears to have two linear regimes, one being dominated by the T_3 component closer to the surface of the gel, and one farther away from the surface, where T_1 contributes most significantly.

Figure 4.25 displays the traction distribution along the same arbitrary plane as in Fig. 4.24 for the next time increment $t_2 = 70$ min. Figure 4.25(a) shows the magnitude of the three-dimensional traction vectors as color contours along the same planar slice, while the white arrows represent the (T_3, T_1) traction components. The color bar displays the units in $pN/\mu m^2$, whereas the magnitude of the longest arrow corresponds to 680 $pN/\mu m^2$. Figure 4.25(b) plots an enlarged picture of Fig. 4.25(a), highlighting an arbitrarily chosen location to generate a line profile of each traction component as a function of depth (x_3), which is shown in Fig. 4.25(c). The traction contours and line profiles show a similar decay with thickness as presented in Fig. 4.24, however, in Fig. 4.25(c) T_3 dominates the total traction vector throughout the entire imaged gel thickness, whereas the in-plane

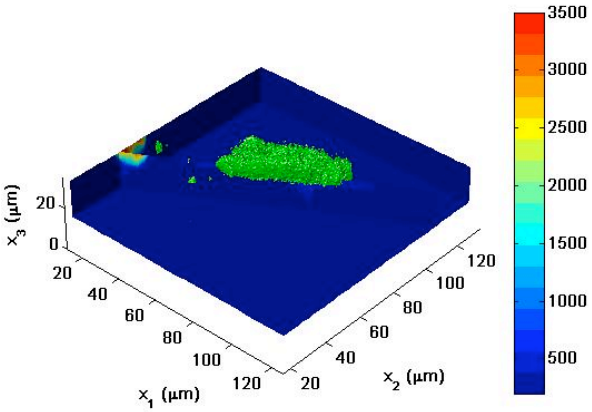

(a) Cell tractions at $t_1 = 35$ min

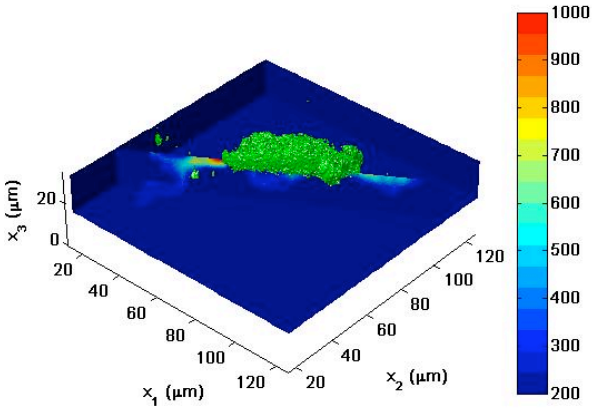

(b) Cell tractions at $t_2 = 70$ min

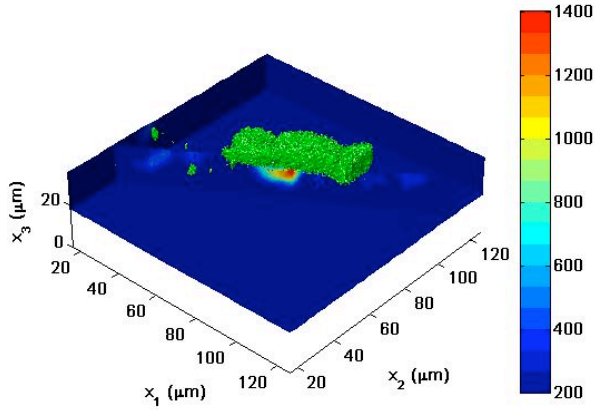

(c) Cell tractions at $t_3 = 105$ min

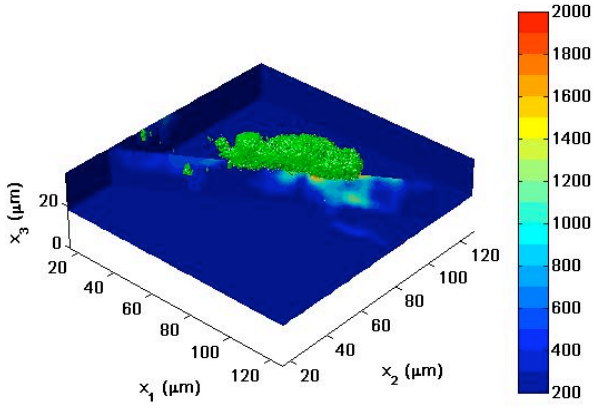

(d) Cell tractions at $t_4 = 140$ min

Figure 4.23: Arbitrary traction contour slices along the long axis of the cell. The color bar indicates the magnitude of the three-dimensional traction vectors along that particular plane in units of $pN/\mu m^2$. The slices of the traction contours underneath migrating cells correspond to the displacement slices shown in Fig. 4.16. The two edges in the image are included to show that there are negligible tractions detected from neighboring cells (contours are dark blue). The cell (green) is superimposed on the three-dimensional contour plots to show its position with respect to the traction field.

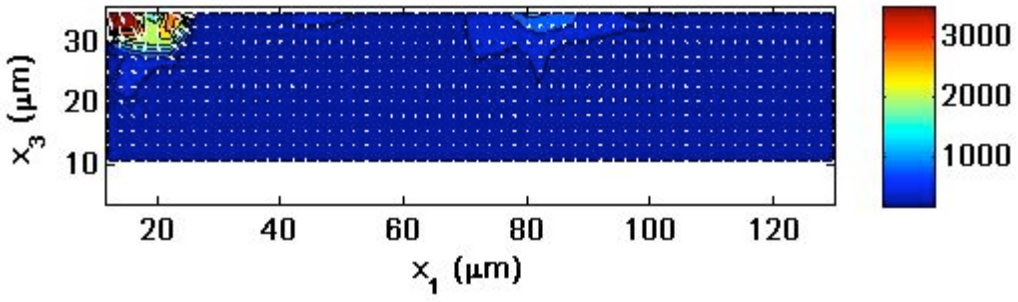

(a) Cross-sectional tractions contour plot through the substrate thickness at $t_1 = 35$ min

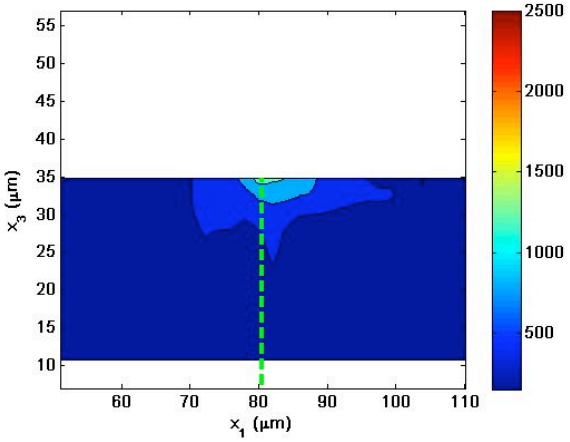

(b) Enlarged view of the contour plot in 4.24(a) and the location of the traction line plot shown in 4.24(c)

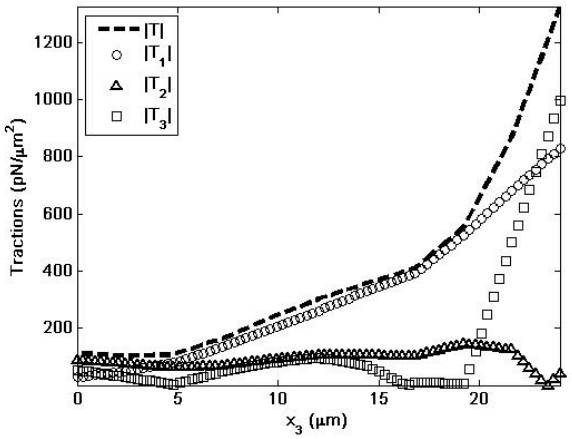

(c) Traction force line profile through the thickness of the gel (x_3). The maximum x_3 value corresponds to the gel surface.

Figure 4.24: Traction contour and line plot profiles as a function of depth (x_3) through the thickness of the gel at time $t_1 = 35$ min. Figure 4.24(a) shows the same traction contours along the long axis of the cell as shown in Fig. 4.23(a), where the color bar represents the magnitude of the three-dimensional traction vectors along that particular plane, and the white arrows show the direction of the in-plane (T_1,T_3) traction components only. Figure 4.24(b) shows the zoom-in image of Fig. 4.24(a), whereas Fig. 4.24(c) illustrates the decay of all traction components and the magnitude of the three-dimensional traction vector in the x_3 direction. All color bar units are $pN/\mu m^2$.

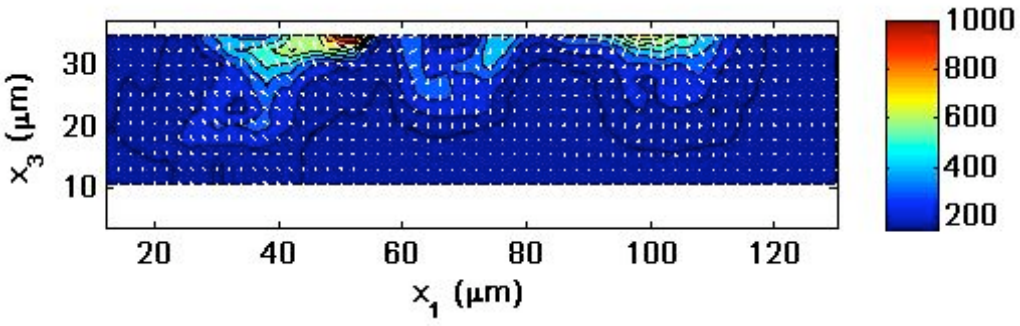

(a) Cross-sectional tractions contour plot through the substrate thickness at $t_1 = 70$ min

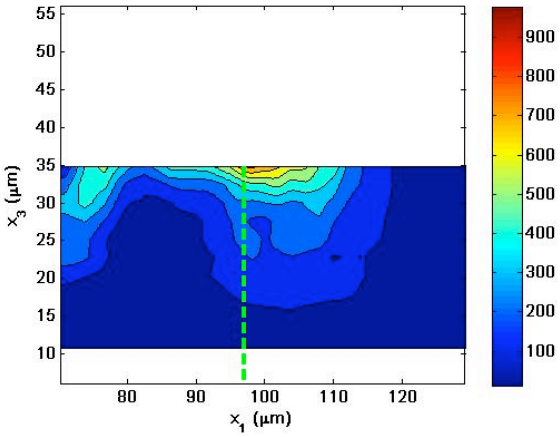

(b) Enlarged view of the contour plot in 4.11(a) and the location of the traction line plot shown in 4.25(c)

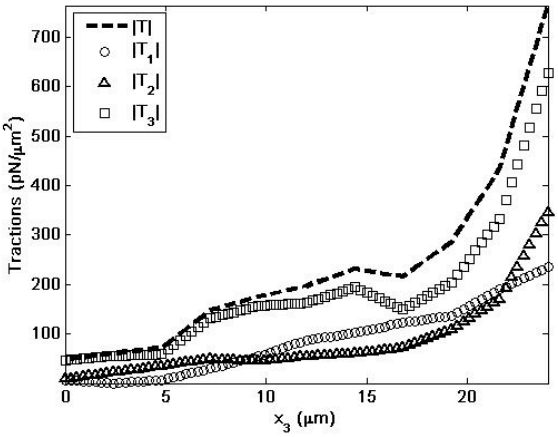

(c) Traction line profile through the thickness of the gel (x_3). The maximum x_3 value corresponds to the gel surface.

Figure 4.25: Traction contour and line plot profiles as a function of depth (x_3) through the thickness of the gel at time $t_2 = 70$ min. Figure 4.25(a) shows the same traction contours along the long axis of the cell as shown in Fig. 4.23(b), where the color bar represents the magnitude of the three-dimensional traction vectors along that particular plane, and the white arrows show the direction of the in-plane (T_1,T_3) traction components only. Figure 4.25(b) shows the zoom-in image of Fig. 4.25(a), whereas Fig. 4.25(c) illustrates the decay of all traction components and the magnitude of the three-dimensional traction vector in the x_3 direction. All color bar units are $pN/\mu m^2$.

components T_1 and T_2 contribute primarily on the surface of the gel to $|\mathbf{T}|$, the magnitude of the total traction vector.

Figures 4.26(a) and 4.27(a) display the surface traction fields presented in Figs. 4.22(a) and 4.22(b) in more detail. In particular, Fig. 4.19(a) shows the magnitude of the three-dimensional traction vectors as color contours directly underneath the migrating cell, while the white arrows represent the (T_1, T_2) traction components. The color bar displays the units in $pN/\mu m^2$, whereas the magnitude of the longest arrow corresponds to 2730 $pN/\mu m^2$. Figure 4.26(b) plots an enlarged picture of Fig. 4.26(a), highlighting an arbitrarily chosen location to generate a line profile of each traction component as a function of spatial distance, which is shown in Fig. 4.26(c). All three traction components display a similar behavior in that they attain there maximum along the same spatial position ($x_1 = 89\ \mu m$).

Figure 4.27(a) shows the same series of plots as Fig. 4.26(a) for the next time increment (t_2 = 70 min). The color contours display the magnitude of the three-dimensional traction vectors underneath the fibroblast, while the white arrows represent the (T_1, T_2) traction components. The color bar displays the units in $pN/\mu m^2$, whereas the magnitude of the longest arrow corresponds to 1000 $pN/\mu m^2$. Figure 4.27(b) plots an enlarged picture of Fig. 4.13(a), highlighting an arbitrarily chosen location to generate a line profile of each traction component as a function of spatial distance, which is shown in Fig. 4.17(c). The line profiles in Figs. 4.17(c) and 4.27(c) were chosen at the leading edge of the motile cell. Comparing the contour plots, and in particular the two line profile plots, Fig. 4.26(c) shows a broader traction profile than Fig. 4.27(c).

Figure 4.28 compares the surface traction fields directly underneath the migrating cells shown in Fig. 4.22(a) and 4.22(b) by highlighting the contribution of the T_3 traction component. Figures 4.28(a) and 4.28(c) show surface contours of the magnitude of the three-dimensional traction vectors whereas Figs. 4.28(b) and 4.28(d) display the magnitude of only the two-dimensional, in-plane (T_1, T_2) traction vectors. Side-by-side comparison reveals that the cell applies mostly in-plane shear tractions (T_1, T_2). Over the course of the shown time increments t_1 and t_2 the contribution of the T_3 traction component as shown in Figs. 4.26(c) and 4.27(c) is relatively insignificant.

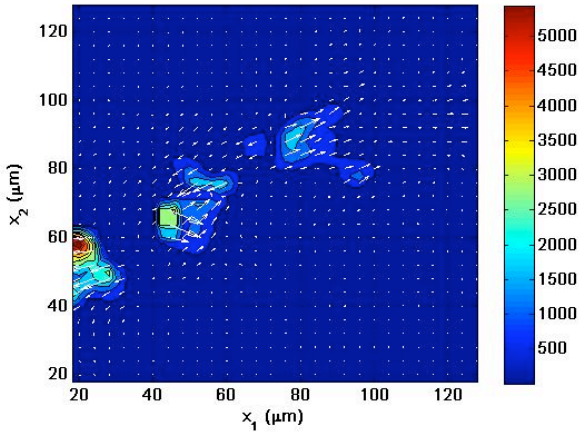

(a) Surface tractions contour plot underneath the migrating cell at $t_1 = 35$ min

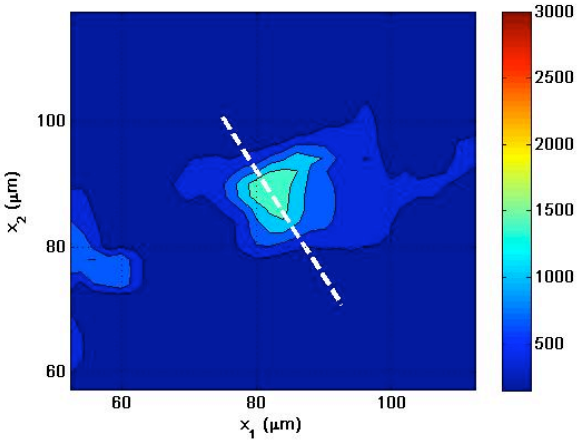

(b) Enlarged view of the contour plot in 4.26(a) and the location of the traction line plot shown in 4.26(c)

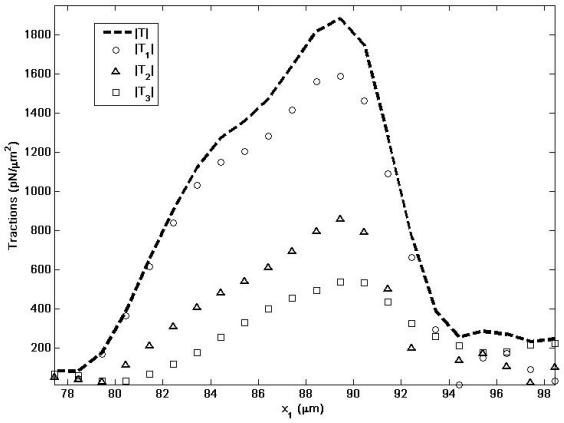

(c) Traction profile along the selected line in 4.26(b)

Figure 4.26: Surface traction contour and line plot profiles along a particular line in the $x_1 - x_2$ top surface plane at $t_1 = 35$ min. Figure 4.26(a) shows the same traction contours as shown in Fig. 4.22(a), where the color bar represents the magnitude of the three-dimensional surface traction vectors and the white arrows show the direction of the in-plane (T_1,T_2) traction components only. The color bar units represent $pN/\mu m^2$. Figure 4.19(b) shows the zoom-in image of Fig. 4.26(a) highlighting the particular region, where the line plot was generated. Figure 4.26(c) illustrates the distribution of all three traction components and the magnitude of the three-dimensional traction vector along the drawn line.

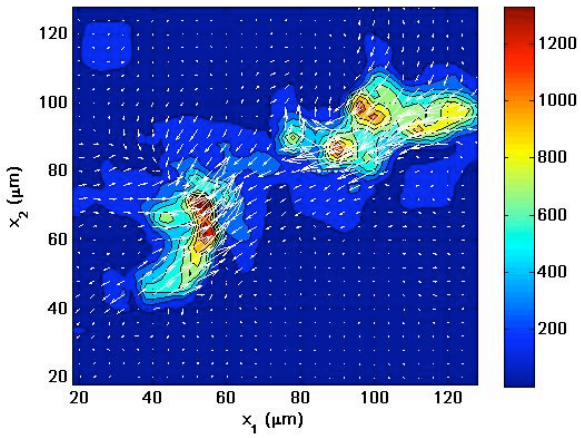

(a) Surface tractions contour plot underneath the migrating cell at $t_2 = 70$ min

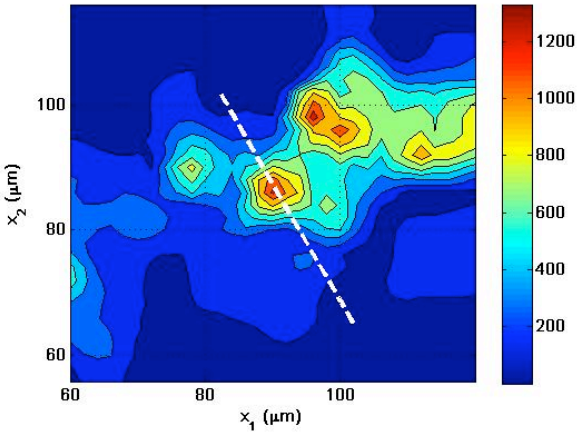

(b) Enlarged view of the contour plot in 4.27(a) and the location of the traction line plot shown in 4.27(c)

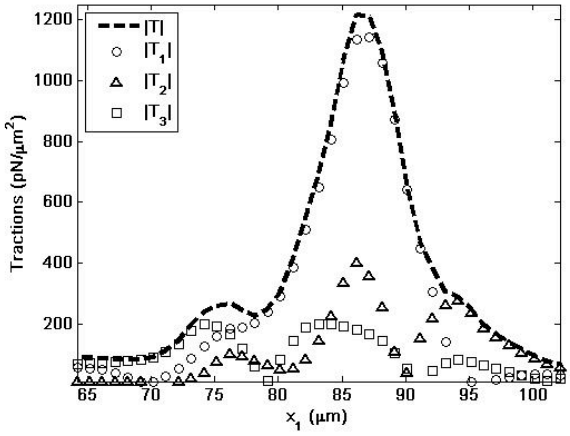

(c) Traction profile along the selected line in 4.27(b)

Figure 4.27: Surface traction contour and line plot profiles along a particular line in the $x_1 - x_2$ surface plane at $t_2 = 70$ min. Figure 4.27(a) shows the same traction contours as shown in Fig. 4.22(b), where the color bar represents the magnitude of the three-dimensional surface traction vectors and the white arrows show the direction of the in-plane (T_1,T_2) traction components only. The color bar units represent $pN/\mu m^2$. Figure 4.6(b) shows the zoom-in image of Fig. 4.27(a) highlighting the particular region, where the line plot was generated. Figure 4.27(c) illustrates the distribution of all three traction components and the magnitude of the three-dimensional traction vector along the drawn line.

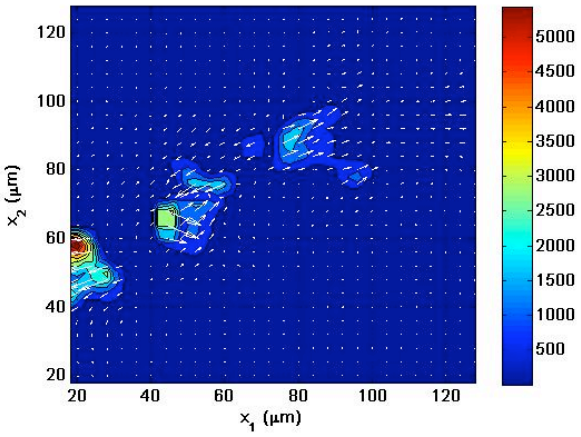

(a) Cell-induced surface tractions (3D) at $t_1 = 35$ min

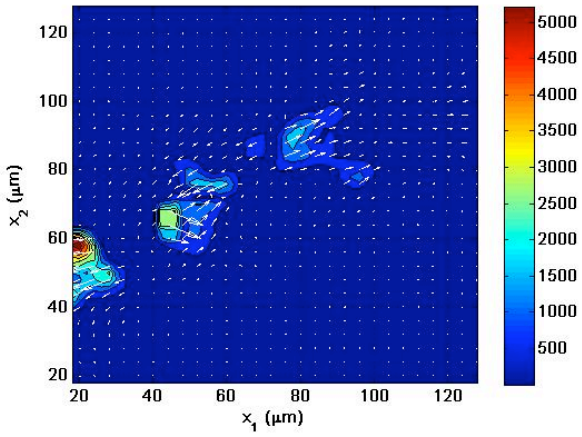

(b) Cell-induced surface tractions (2D) at $t_1 = 35$ min

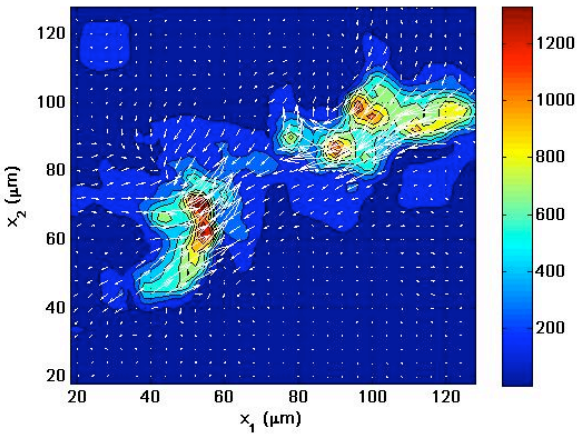

(c) Cell-induced surface tractions (3D) at $t_2 = 70$ min

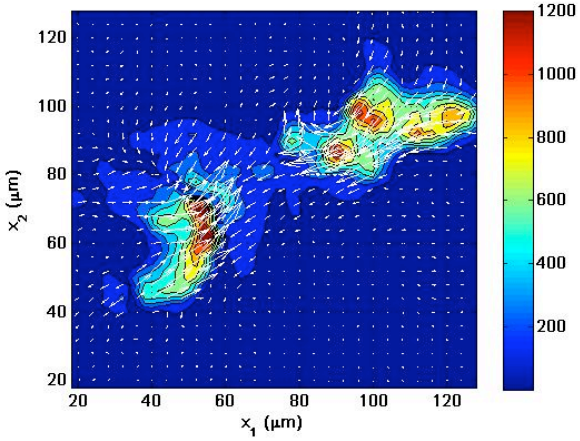

(d) Cell-induced surface tractions (2D) at $t_2 = 70$ min

Figure 4.28: Comparison between the magnitude of the three-dimensional traction vector (4.28(a) and 4.28(c) and the magnitude of the two-dimensional traction vector (T_1, T_2) components only (4.28(b) and 4.28(d))). The color bar is displaying all traction values in $pN/\mu m^2$, and and the white arrows show the direction of the in-plane (T_1,T_2) traction components only.

4.6 Inhibiting Cell Contractility and Cell Locomotion

In order to conclude that the experimentally observed displacements are indeed caused by cell-mediated forces, cell displacements were monitored before and after the cells were treated with a myosin II blocker. This blocker protein, blebbistatin (Sigma-Aldrich, St. Louis, MO), inhibits the myosin II molecular motor proteins from moving along the cell's actin filaments to cause cytoskeletal contraction. Blebbistatin is commonly used in traction or traction force measurements to inhibit actomyosin contraction in non-muscle cells [5, 6]. If the cell is unable to generate actomyosin based internal forces that are transmitted through focal adhesions to the substrate, then there should be be no evident substrate displacements. Hence, this experiment serves as a validation tool that the previously observed displacements are in fact cell-mediated, and are not due to thermal fluctuation or instrument noise. Confocal stacks of individual cells were captured 1-2 hours before treatment with 12.5 μM blebbistatin, and up to 4 hours post-treatment. Figures 4.29(a) - 4.29(d) show the resulting surface displacement fields before and after blebbistatin injection as displacement contours. The contours represent the magnitude of the three-dimensional displacement vectors, whereas the white arrows indicate the in-plane (u_1,u_2) displacements only. The color bar is indicating all values in μm. Figure 4.29(e) shows the average maximum surface displacements achieved by a single cell at time points before and after blebbistatin injection. Following the treatment, there is a notable decrease in the average maximum displacement. Despite the cell's presence, there are no detectable displacements after 35 minutes. Identical experiments performed without cells and in the presence of blebbistatin yielded no notable displacements, establishing that all measured displacements are cell-induced.

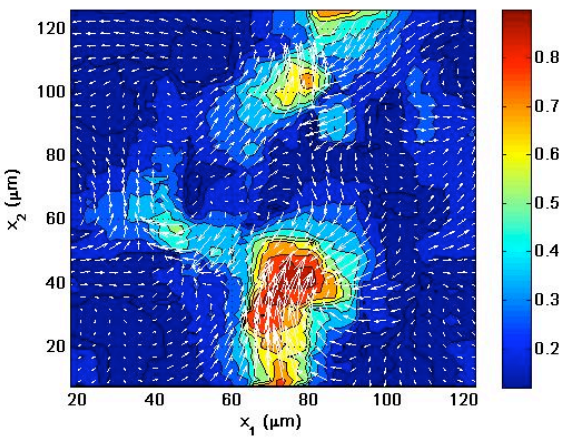

(a) Cell-induced surface displacements before blebbistatin treatment

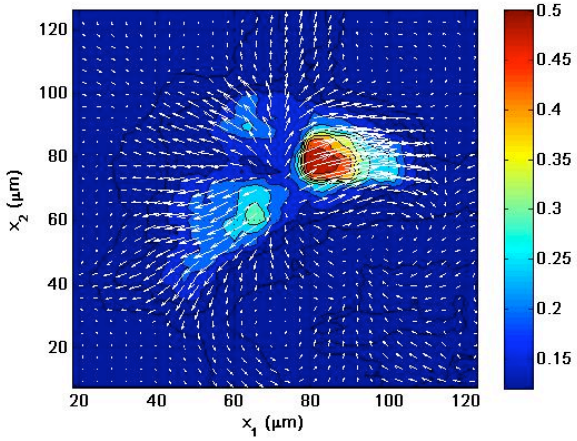

(b) Cell-induced surface displacements at blebbistatin injection

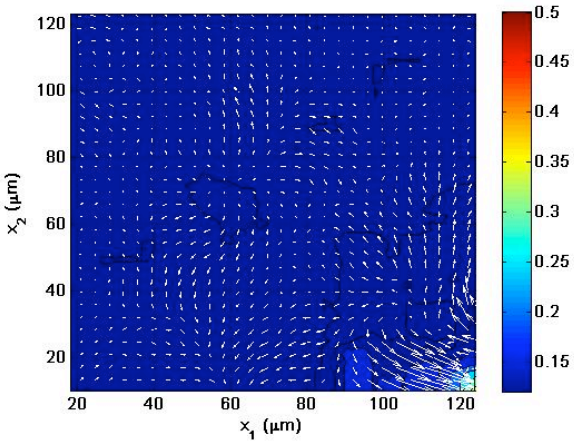

(c) Cell-induced surface displacements 35 min after treatment

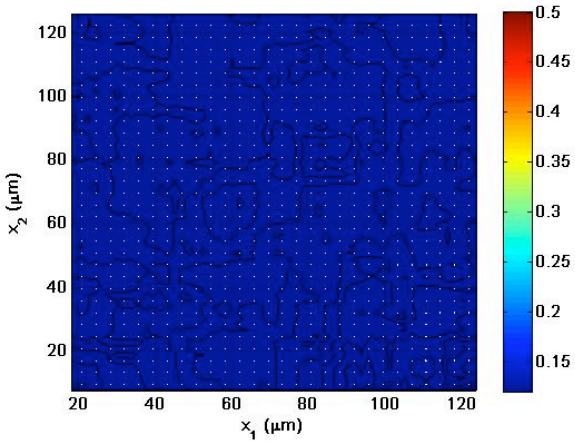

(d) Cell-induced surface displacements 245 min after treatment

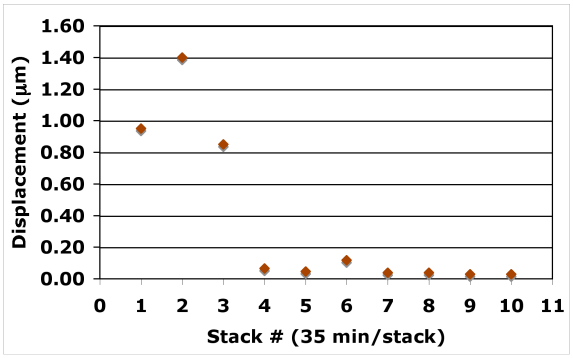

(e) Plot of the average maximum observed cell-induced surface displacement before and after treatment with blebbistatin. (blebbistatin injection occured at stack #3.)

Figure 4.29: Successive time series of cell-induced surface displacements before (4.29(a) and 4.29(b)) and after treatment with blebbistatin (4.29(c) and 4.29(d)). Color contours display the magnitude of the three-dimensional displacement vector, while the white arrows show the direction of the in-plane (u_1,u_2) displacement components only. The color bar represents all values in μm.

4.7 Comparison of Cell Response on Soft and Stiff Substrates

Comparing the magnitude of the measured displacement fields on *soft* and *stiff* substrates shows similar values (same order of magnitude) during cell migration, suggesting that the cell actively regulates the amount of force needed to generate enough surface displacements. Figures 4.30 and 4.31 show that while the magnitudes of the surface displacement on *soft* and *stiff* substrates display values of the same magnitude order, the tractions are different by approximately a factor of ten. The ratio of the *soft* and *stiff* substrate material Young's moduli is also approximately ten, which suggests that the cell tractions scale linearly with the Young's moduli of the substrates studied here. This trend is noticable throughout all of the experiments performed on both substrates, and this scaling behavior has been observed previously [3].

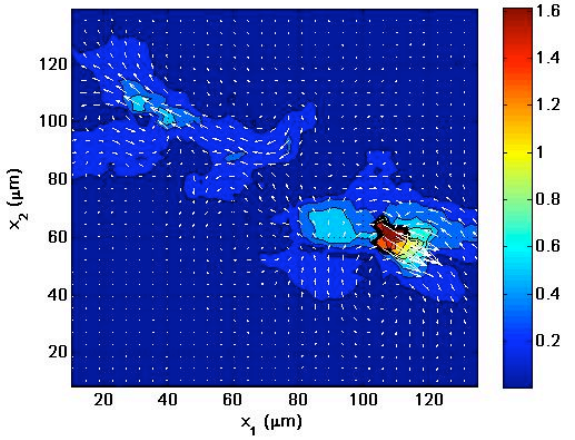

(a) Cell-induced surface displacements on *soft* polyacrylamide gels at $t_1 = 35$ min

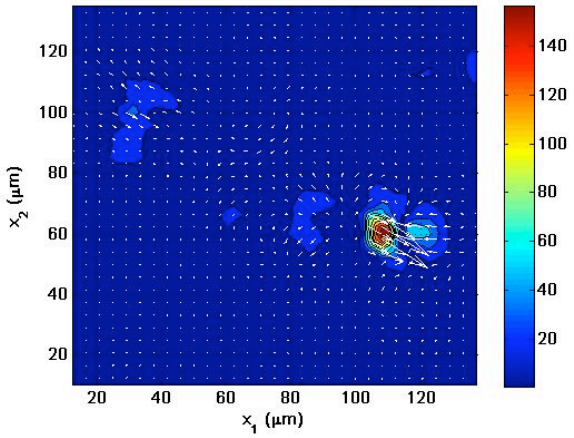

(b) Cell-induced surface tractions on *soft* polyacrylamide gels at $t_1 = 35$ min

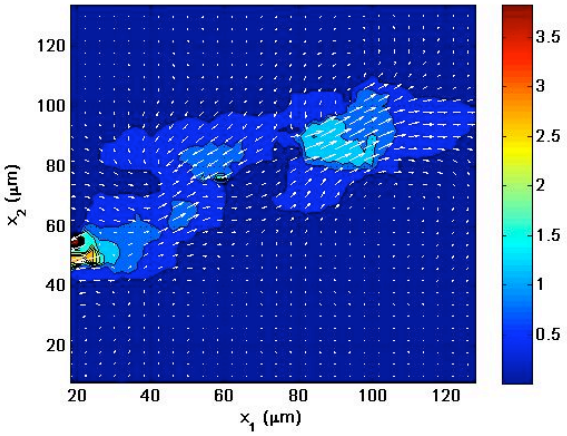

(c) Cell-induced surface displacements on *stiff* polyacrylamide gels at $t_1 = 35$ min

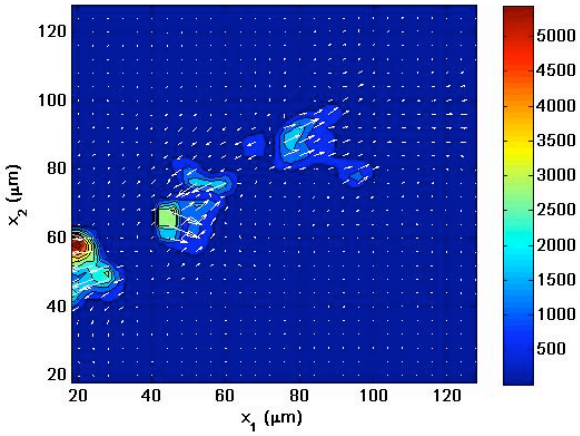

(d) Cell-induced surface tractions on *stiff* polyacrylamide gels at $t_1 = 35$ min

Figure 4.30: Comparison between the three-dimensional cell induced surface deformation on *soft* (4.31(a) and 4.31(b)) and *stiff* (4.31(c) and 4.31(d)) polyacrylamide gel substrates for a 35 min time increment. The color bar in Figs. 4.31(a) and 4.31(c) indicates all values in μm, whereas the color bar in Figs. 4.31(b) and 4.31(d) displays all values in $pN/\mu m^2$. The Young's moduli of the *soft* and *stiff* substrates are 0.82 and 9.64 kPa, respectively.

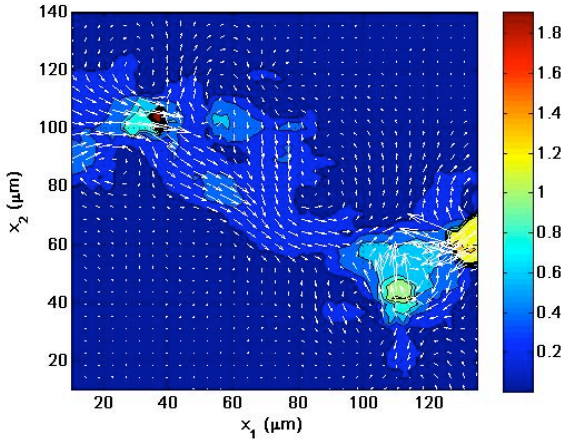

(a) Cell-induced surface displacements on *soft* polyacrylamide gels at $t_1 = 70$ min

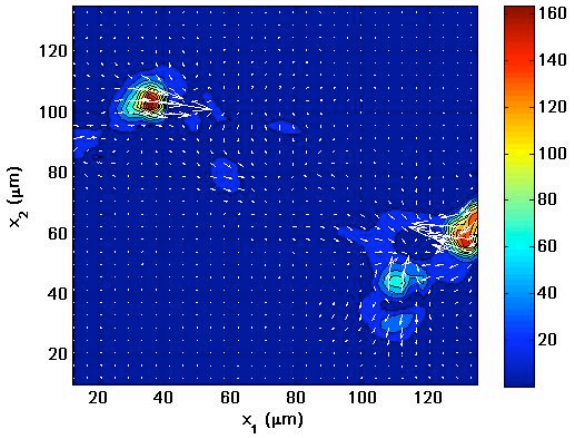

(b) Cell-induced surface tractions on *soft* polyacrylamide gels at $t_1 = 70$ min

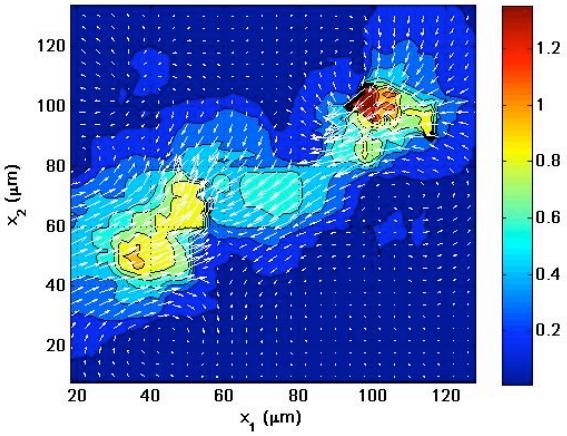

(c) Cell-induced surface displacements on *stiff* polyacrylamide gels at $t_1 = 70$ min

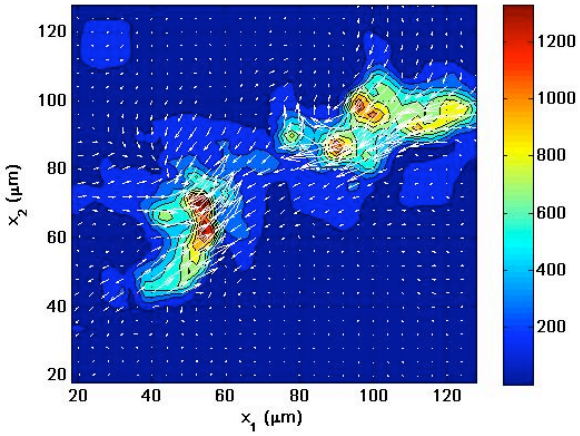

(d) Cell-induced surface tractions on *stiff* polyacrylamide gels at $t_1 = 70$ min

Figure 4.31: Comparison between the three-dimensional cell induced surface deformation on *soft* (4.31(a) and 4.31(b)) and *stiff* (4.31(c) and 4.31(d)) polyacrylamide gel substrates for a 35 min time increment. The color bar in Figs. 4.31(a) and 4.31(c) indicates all values in μm, whereas the color bar in Figs. 4.31(b) and 4.31(d) displays all measurements in $pN/\mu m^2$. The Young's moduli of the *soft* and *stiff* substrates are 0.82 and 9.64 kPa, respectively.

4.8 Implications of Three-dimensional Measurements for Current Cell Motility Models

The deformation results presented in Sections 4.2 - 4.5 highlight the strong three-dimensional dependence of cell-matrix interactions during cell migration. One important implication of these findings is in the context of cell motility models that are typically based on existing two-dimensional cell displacement and traction or traction force data. This section briefly reviews the basis of the most widely accepted motility model based on two-dimensional experimental data, and gives an outlook on a potential new cell migration mechanism based on the three-dimensional experimental observations presented here. It should be noted however, that the suggested migration mechanism outlined here is based on the results presented in the previous sections, and additional experiments are necessary to elucidate this further.

One of the most commonly accepted cell motility models describes the process of cell motion in four general steps, as illustrated in Fig. 4.32. The following is a summary of these steps, and further detailed information can be found elsewhere [2, 1]. The first step, as shown in Fig. 4.32(a), consists of the protrusion of actin fibers at the leading edge via actin polymerization. Typically, actin polymerization rates vary and can be different at either end leading to differential polymerization or treadmilling. This allows the cell to actively control the shape of its cytoskeleton. Next, the newly formed protrusion will engage the substrates through ligand-receptor connection (Fig. 4.32(b)), which generally involve the interplay of many focal adhesion proteins. This newly formed adhesion anchor site, or focal adhesion complex, will be utilized later by the cell to transmit forces to the substrate or matrix material. In step three, as shown in Fig. 4.32(c), the cell detaches from the trailing edge by possibly disassembling the focal adhesion complex. Finally, the cell generates an internal contractile force by the activation of actomyosin, and due to the imbalance of forces, propels itself forward, as illustrated in Fig. 4.32(d).

While this description of cell movement is oversimplified, the basic cell-generated tractions responsible for cell motion are thought to be only planar. However, as shown in the previous sections,

cell-induced displacements and tractions are not only planar but rather highly three-dimensional. This is further illustrated in Fig. 4.33, where the cell seems to undergo a sort of peeling or rolling motion during its movement from left to right. The leading edge of the cell is located towards the right end of the Fig., whereas the trailing edge is located towards the left end (also, see Figs. 4.15 - 4.23). The Fig. illustrates the progression of the in-plane (T_1) and normal (T_3) shear tractions underneath the long axis of the cell along the same arbitrarily selected slice as presented in Sections 4.4 and 4.5. The color contours display the magnitude of the three-dimensional traction vector, while the black arrows indicate the (T_1, T_3) shear traction components. The time series shows the evolution of the substrate shear tractions as the cell moves from the left to the right, suggesting a potential peeling mechanism. Examining the magnitude of each of the T_1 and T_3 components in Fig. 4.34 elucidates this mechanism in more detail. The in-plane (T_1) tractions seem to alternate between local contraction and extension close to force equilibrium, while the normal (T_3) tractions show a net moment around the center of the cell body in Figs. 4.34(a) and 4.34(e). This implies the cell is utilizing a more complex migration mechanism than previously thought, incorporating out-of-plane (normal) rotations along with in-plane contractions and extensions. Previous cell motility models primarily focused on the in-plane forces due to the lack of information in the third dimension, thus suggesting a purely in-plane "push-pull" hypothesis.

A potential analog to this observed mechanism is the rapid attachment and detachment of individual setae of a gecko's toe. These animals have the ability to generate large frictional and adhesion forces to climb steep inclines and vertical walls using van der Waals interactions between their spatulae that comprise the setae and the substrate material [50]. During the approach stage, the gecko's spatulae adhere to the substrate in an almost parallel configuration with minimal adhesive force. Then, the gecko "rolls" and "grips" its toes inward generating large frictional (in-plane) and adhesion (normal) forces. The final step involves a "rolling-out" process, in which the gecko peels its spatulae off the substrate surface from rear to front. The experimental findings presented here reveal new insights into the cell's complex migration machinery and should provide an impetus for the development of new three-dimensional cell motility models.

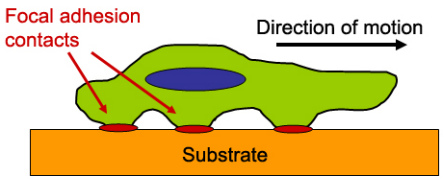

(a) Protrusion of the leading edge through actin polymerization

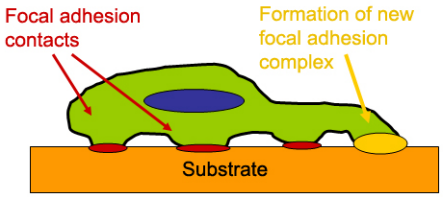

(b) Adhesion at the leading edge

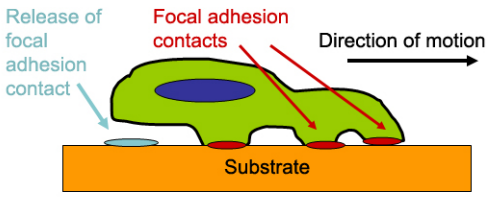

(c) Detachment at the trailing edge

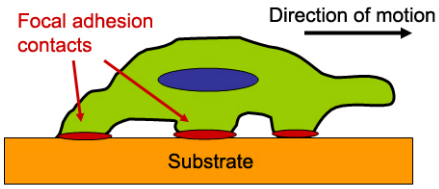

(d) Cell contraction and movement of the cell body

Figure 4.32: A schematic of the four basic steps involved in cell motion. Movement is initiated by the protrusion of the the cystoskeleton by actin polymerization 4.32(a) followed by formation of focal adhesion complexes and adhesion to the substrate 4.32(b). Next, the cell detaches its trailing edge from the substrate 4.32(c) and finally generates an internal force to contract and propel itself forward 4.32(d).

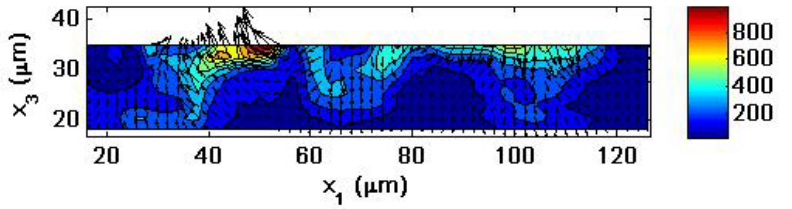

(a) Cell-induced shear tractions at $t_2 = 70$ min

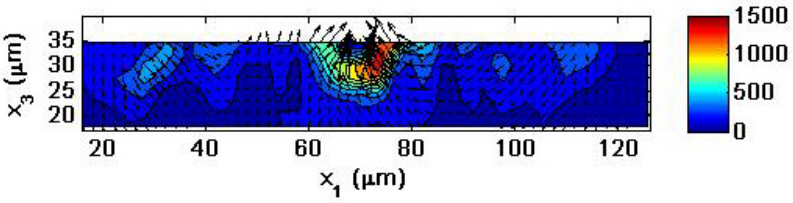

(b) Cell-induced shear tractions at $t_3 = 105$ min

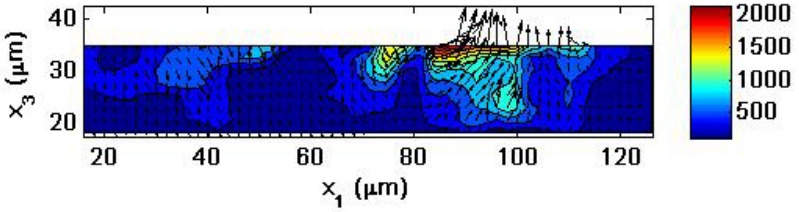

(c) Cell-induced shear tractions at $t_4 = 140$ min

Figure 4.33: Time evolution of cell-induced tractions as a function of depth (x_3) over 70 min along an arbitrary slice below the cell's long axis. The contour plots show the magnitude of the three-dimensional traction vector as previously plotted in Figs. 4.24(a) - 4.25(a). The black arrows represent the in-plane shear tractions (T_1, T_3), where the magnitude of the longest arrow in each Fig. is equal to the maximum value depicted by the color bar in $pN/\mu m^2$. The particular time increments that are shown here are t_2, t_3, and t_4, where the time increment between each frame is 35 min. The leading edge of the cell is located on the right ($\sim x_1 = 120$ μm), and the direction of cell migration is from left to right.

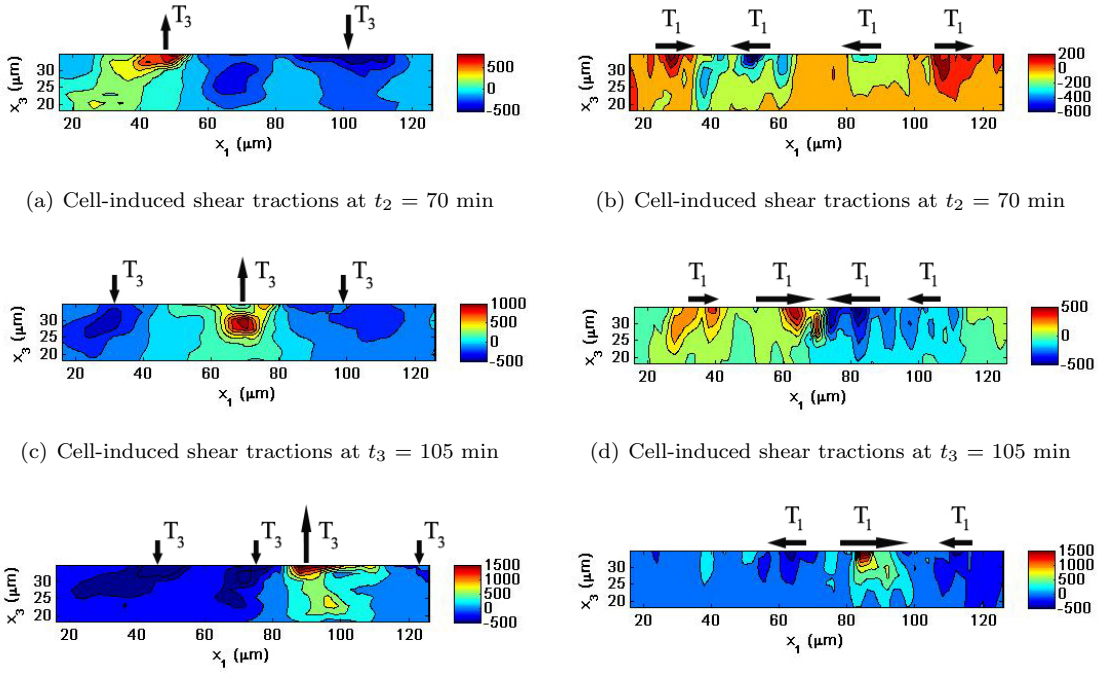

(a) Cell-induced shear tractions at $t_2 = 70$ min

(b) Cell-induced shear tractions at $t_2 = 70$ min

(c) Cell-induced shear tractions at $t_3 = 105$ min

(d) Cell-induced shear tractions at $t_3 = 105$ min

(e) Cell-induced shear tractions at $t_4 = 140$ min

(f) Cell-induced shear tractions at $t_4 = 140$ min

Figure 4.34: Time evolution of cell-induced shear tractions (T_1, T_3) as a function of depth (x_3) over 70 min along an arbitrary slice below the cell's long axis. The contour plots show the magnitude of the shear traction components (left column: T_3; right column: T_1). The color bar units are $pN/\mu m^2$. The black arrows on the top of each plot give the general direction of the cell-generated tractions. The particular time increments that are shown here are t_2, t_3, and t_4, where the time increment between each frame is 35 min. The leading edge of the cell is located on the right ($\sim x_1 = 120$ μm), and the direction of cell migration is from left to right.